3D model of mouse embryonic pancreas and endocrine compartment using stem cell-derived mesoderm and pancreatic progenitors

Shlomit Edri[1*], Vardit Rosenthal[1], Or Ginsburg[1], Abigail Newman Frisch[1], Christophe E. Pierreux[2], Nadav Sharon[3] and Shulamit Levenberg[1*]

[1]Faculty of Biomedical Engineering, Technion – Israel Institute of Technology, Haifa, Israel

[2]Cell Biology Unit, de Duve Institute, UCLouvain, Woluwe, Belgium

[3]Faculty of Biology, Technion – Israel Institute of Technology, Haifa, Israel

*Corresponding authors: Shlomit Edri: shlomitedri@campus.technion.ac.il and Shulamit Levenberg: shulamit@bm.technion.ac.il

Abstract

The developing mouse pancreas is surrounded by mesoderm compartments providing signals that induce pancreas formation. Most pancreatic organoid protocols lack this mesoderm niche and only partially capture the pancreatic cell repertoire. This work aimed to generate pancreatic aggregates by differentiating mouse embryonic stem cells (mESCs) into mesoderm progenitors (MPS) and pancreas progenitors (PPs), without using extracellular matrix substitutes. First, mESCs were differentiated into epiblast stem cells (EpiSCs) to enhance the PP differentiation rate. Next, PPs and MPs aggregated together giving rise to various pancreatic cell types, including endocrine, acinar, and ductal cells, and to endothelial cells. Single-cell RNA sequencing analysis revealed a larger endocrine population within the PP+MP aggregates, as compared to PPs alone or PPs in Matrigel aggregates. The PP+MP aggregate gene expression signatures and its endocrine population percentage closely resembled those of the endocrine population found in the mouse embryonic pancreas, which holds promise for studying pancreas development.

Introduction

The pancreas is a gland with two main compartments, exocrine and endocrine, which are essential for digestion and glucose homeostasis, respectively. Its endocrine function is achieved through the release of glucagon and insulin, two major hormones produced by alpha and beta cells, respectively, and which are required to maintain normal blood glucose levels. The exocrine compartment is composed of acinar cells, which synthesize, store and secrete enzymes, such as trypsin, amylase and lipase that break down proteins, carbohydrates and fats. These digestive enzymes drain into the duodenum via a highly branched network of ducts within the pancreas [1,2].

In early stage of development, mammalian embryos undergo gastrulation in which a single layered hollow sphere of cells reorganizes into a multi-layered structure. The primary function of gastrulation is to generate an axial system, to correctly position the germ layers in relation to one another for subsequent morphogenesis and to generate the mesoderm [3] (Fig. S1A). In mammalian embryos, the pancreas develops from the gut tube endoderm in a region proximal to the notochord, paired dorsal aortas artery and ventral vitelline veins which all derive from the mesoderm (Fig. S1B). The mesoderm-derived cells (Fig. S1A-B) are important for generating the signals and mechanical constraints that induce the formation of the pancreatic bud and its later differentiation [4,5].

Pluripotent stem cells (PSCs) serve as a good model for the study of pancreas organogenesis, since they recapitulate the dynamic expression of key genes involved in this developmental process. Figure S1C provides a visual presentation of the trajectory of PSCs during in vitro differentiation, showcasing the

different stages and key genes expressed in each state. The information was derived from studies investigating murine pancreas development and the differentiation of human PSCs towards pancreatic identity [6–9]. PSCs are first differentiated to definitive endoderm (DE), which gives rise to many of the body's internal organs. After several differentiation stages, the DE finally differentiates into multipotent pancreatic progenitors (PPs) coexpressing Pdx1 and Nkx6-1. PPs can generate the various pancreatic cell types by further differentiating into acinar, duct and endocrine progenitors [10–12]. These, in turn, can be applied to form organoids, which are three-dimensional (3D) in vitro models of stem cells or organ-specific progenitors that have the capacity to self-organize into specific structures that display architectures and functionalities similar to in vivo tissues and organs [13]. In addition to these interesting and promising similarities, organoids can be generated in large numbers, thereby offering the possibility to a diversity of manipulation. In the past decade, pancreatic organoids have drawn the attention of researchers due to their considerable potential in the study of pancreas development, disease modelling, drug testing and cellular therapy.

Several protocols have been developed for the generation of pancreatic organoids from human PSCs ([12,14–19] and reviewed in [20]). Although, mouse pancreatic organoids have also been generated from cells isolated from either adult or embryonic pancreatic tissue [21–23], mouse PSC-based models are less commonly used. During organoid fabrication, single cells or cell clusters are embedded in Matrigel, which provides mechanical support and serves as an extracellular matrix (ECM) substitute [21–23]. However, the composition of Matrigel, which is a mouse tumour-derived basement membrane ECM [24], suffers from batch-to-batch variability, thus rendering it is suboptimal for reproducible and complete studies focusing on cell self-organization process and signals during organogenesis [25,26]. Furthermore, this tumour-derived ECM has limited clinical translational potential [26,27].

Pancreatic organoids, either PSC-derived or tissue-derived organoids, are limited in their ability to fully recapitulate tissue differentiation. They also fail to reconstruct the mesoderm niche surrounding the developing pancreas. These pancreatic organoids usually lack specialized cell types, such as endothelial and mesenchymal support cells. Although there have been instances where differentiation of human PSCs into beta cells occurred along with the emergence of non-endocrine cells resembling exocrine and mesenchymal cells [28], such models are rare. To overcome these limitations, this work aimed to assemble a reproducible, well-defined 3D pancreatic system that recapitulates the development of the pancreas with its microenvironment. To ensure comparability of the new in vitro model with the embryonic pancreas, the initial pluripotency state of the mouse embryonic stem cells (mESCs) was assessed prior differentiation to achieve optimal pancreatic differentiation. In addition, the system integrated mesoderm to enable development of a pancreatic niche, and Matrigel usage was avoided. The work attempted to advance mESCs to epiblast stem cells (EpiSCs), then differentiate them and later form a tissue-like environment in which EpiSC-derived PPs are in contact with EpiSC-derived mesoderm progenitors (MPs). The mouse model enabled a comparative analysis by single-cell RNA sequencing (scRNA-seq) between the mouse EpiSC-derived pancreatic aggregates and the mouse embryo pancreas at various embryonic stages, which revealed the presence of various pancreatic lineages in the in vitro system. Furthermore, the single cell transcriptome in vitro – in vivo systems' comparison enabled a deeper understanding of the limitations inherent to studying pancreas development in vitro.

Results

In vitro differentiation of EpiSCs to PPs passes through a rich definitive endoderm stage and results in high cell yield

mESCs differentiation usually starts when the cells are grown in the presence of either serum and leukemia inhibitory factor (LIF) [29–31] or 2i, a cocktail of two inhibitors of ERK and GSK3 [32–34]. mESCs cultured in serum and LIF (referred to as SL) or in 2i are referred to as cells in a naïve or naïve ground

88 state, respectively. Specifically, it has been shown that differentiation to pancreatic lineages started
89 when mESCs were in a naïve state [35,36]. The majority of works on PSCs differentiating to pancreas lineage
90 showed advances in differentiating human PSCs [12,36–38]. It has been demonstrated that human
91 embryonic stem cells (ESCs) and human induced PSCs (iPSCs) exhibit greater similarities to mouse
92 epiblast stem cells, primed PSCs, rather than to ESCs at naïve or ground states. Both human PSCs and
93 mouse EpiSCs correspond to post-implantation epiblast and share similar morphology, signalling
94 pathway, metabolism and epigenetic patterns [39–42] (Fig. 1A). This led to the postulation that advancing
95 mESCs to EpiSCs can improve the efficacy of their differentiation to pancreatic progenitors, relying on
96 the field advances in human PSCs differentiation. Accordingly, the response of mESCs in different states
97 of pluripotency to pancreatic differentiation cues was examined (Fig. 1A and Methods). mESCs in naïve
98 and in ground states and EpiSCs were subjected to a 14-day differentiation protocol based on a human
99 PSC-to-PP protocol [12]. At baseline, cells in the three starting conditions shared expression of the core
100 pluripotency factors Oct4, Nanog and Sox2 (Fig. 1B). Cells grown in 2i and SL expressed higher levels of
101 Nanog and Sox2 in comparison to EpiSCs, which also expressed the epiblast-specific gene Fgf5 that was
102 absent in mESCs (Fig. 1B and [43]).

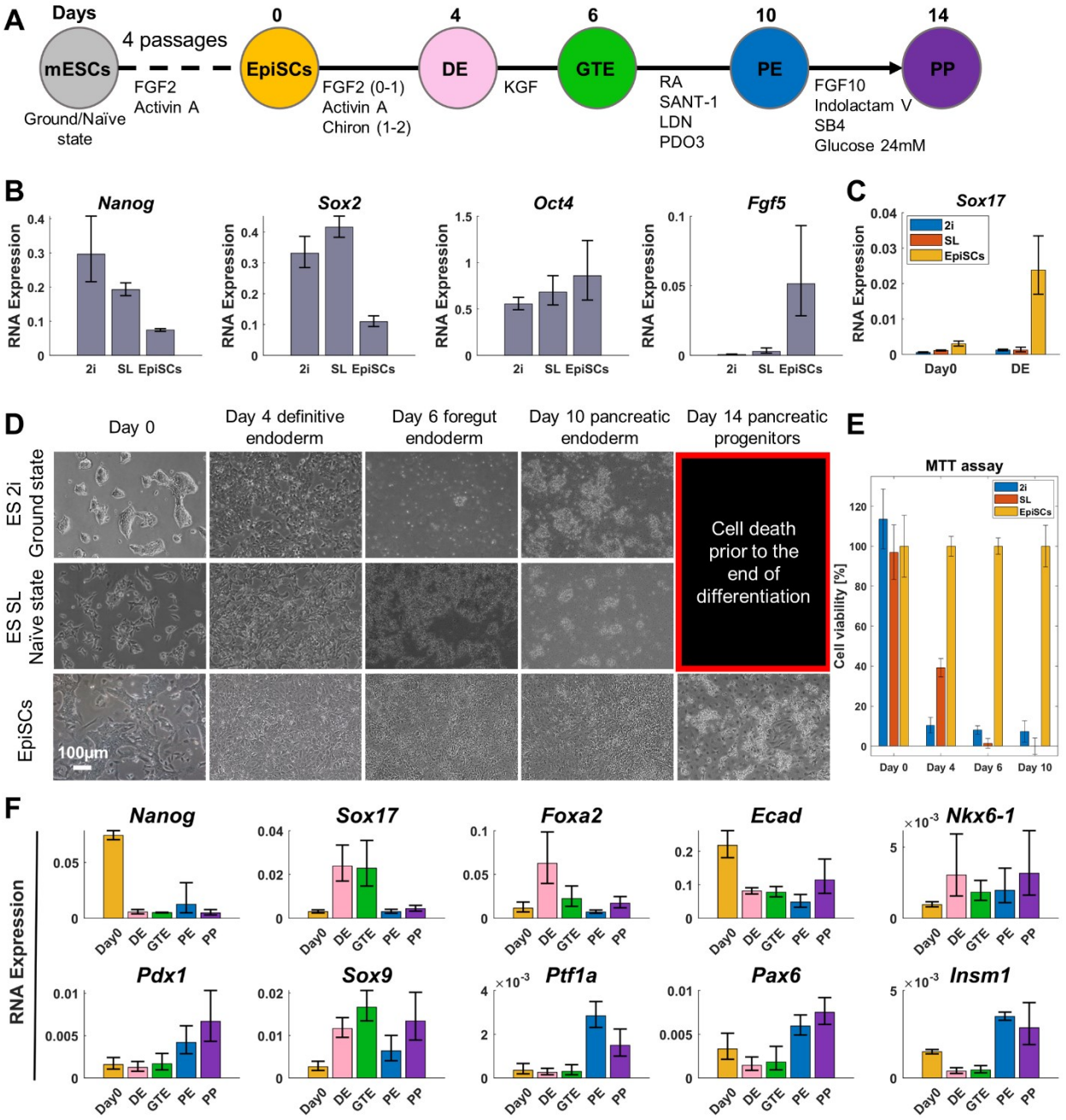

Figure 1. EpiSCs are a better source than ESCs for PP differentiation. A. In vitro differentiation course of mouse PSCs. The differentiation started either from mESCs at ground state (ES 2i), naïve state (ES SL) or EpiSCs. **B.** Relative RNA expression obtained by RT-qPCR of the three pluripotency states prior differentiation. Cells expressed the pluripotency markers Nanog, Sox2 and Oct4. Data are presented as mean±SEM, n=3 biological experiments. **C.** Sox17 expression, as measured by RT-qPCR, of cells at different initial pluripotency states during the differentiation at day 0 and day 4 referred to as definitive endoderm stage. Data are presented as mean±SEM, n=3 biological experiments. **D.** Cell morphology along the course of differentiation. **E.** Cell viability, as measured using the MTT assay, expressed as the percentage of total EpiSCs at each time point along the course of differentiation. Data are presented as mean±SEM, n=7 replicates. **F.** Relative RNA expression of pluripotency, endoderm and pancreatic gene markers during EpiSC differentiation to PPs, as measured by RT-qPCR. Data are presented as mean±SEM, n=3 biological experiments. mESCs, mouse embryonic stem cells; EpiSCs, epiblast stem cells; DE, definitive endoderm; GTE, gut tube endoderm; PE, pancreatic endoderm; PP, pancreatic progenitor.

116 ESCs starting their differentiation in 2i and SL growth medium, exhibited significantly lower expression of
117 Sox17 on differentiation day 4 (DE stage), in comparison to ESCs which first transitioned to EpiSCs (Fig. 1C).
118 Furthermore, ESCs starting their differentiation in 2i and SL growth medium, underwent cell death at around
119 differentiation day 6 (Fig. 1D-E). In contrast, when the differentiation began after ESCs transitioned to EpiSCs,
120 cells survived longer and a higher cell yield was obtained by the end of the differentiation period (Fig. 1D-E).
121 Thus, it was concluded that EpiSCs are superior to naïve ESCs for endoderm and specifically pancreas
122 differentiation, which led further investigation of EpiSC differentiation to PPs.
123 Along the course of EpiSC differentiation, mRNA expression (Methods and Fig. 1F) of the pluripotent markers
124 Nanog and Ecad decreased, whilst the endodermal markers Sox17 and Foxa2 reached their highest levels at
125 the DE and GTE stages (days 4 and 6, respectively). As the differentiation continued, Ecad expression
126 remained constant between DE and PPs and there was a rise in the expression of pancreatic markers (Pdx1,
127 Nkx6-1, Sox9, Ptf1a, Pax6, Insm1), mostly at PE and PP stages (days 10 and 14, respectively). At the protein
128 level (Methods, Fig. 2 and Fig. S2), there was an elevation of pancreatic markers and a reduction in Sox17
129 (endoderm) and in non-pancreas endoderm lineage markers (liver, lung, stomach and intestine, see Fig. S2)
130 at the end of differentiation. Moreover, on differentiation day 14, most of the cells coexpressed SOX9/PDX1
131 and over 86% of the cells coexpressed PDX1 and NKX6-1, indicating a highly efficient PP differentiation
132 protocol (Fig. 2C and Fig. S3).

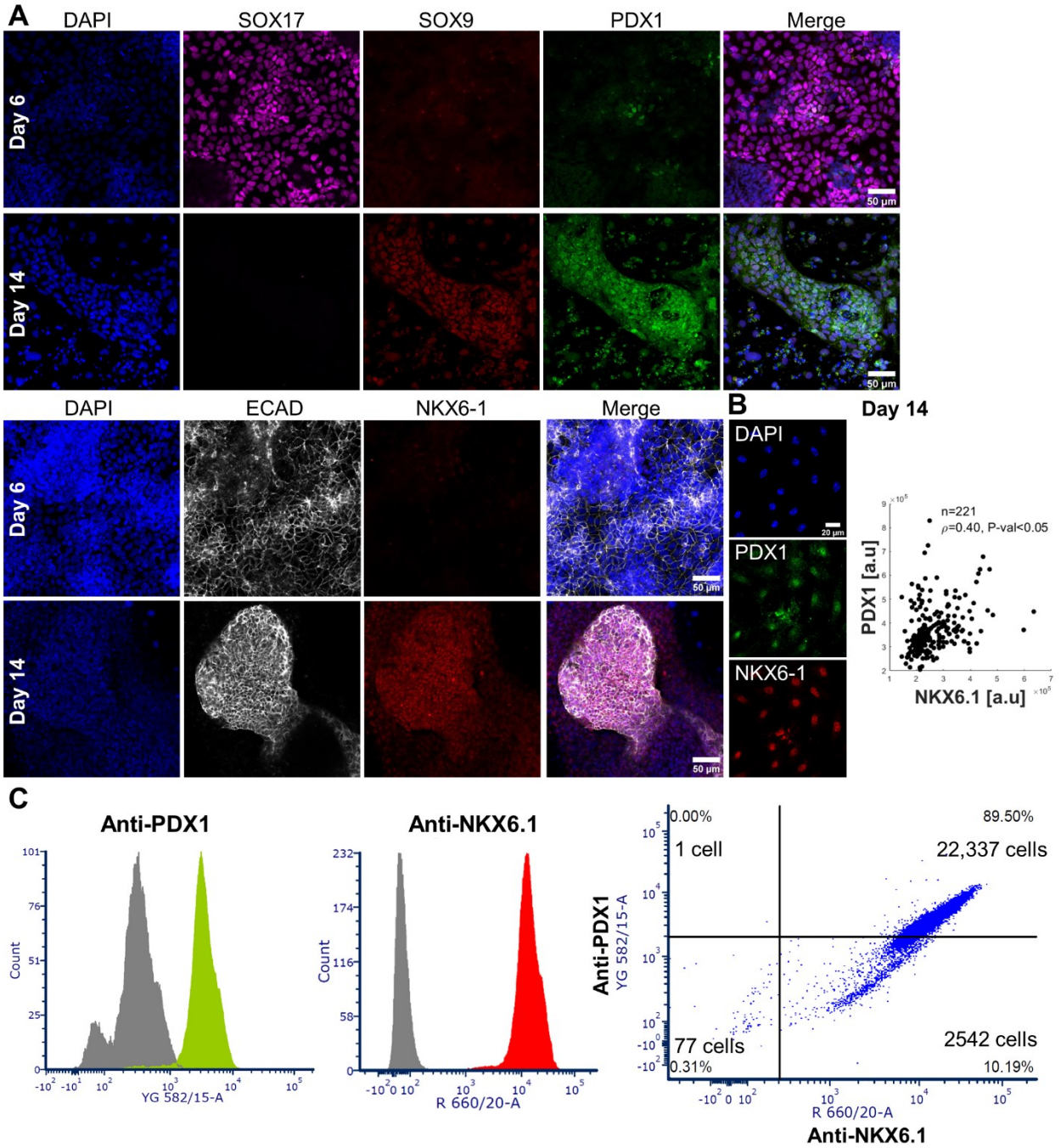

Figure 2. The majority of pancreatic progenitors derived from epiblast stem cells coexpressed PDX1 and NKX6-1. A. Confocal images captured along the course of EpiSC differentiation (day 6, i.e., the gut tube endoderm stage and day 14, i.e., the pancreatic progenitor stage at the end of the differentiation). The cells were immunofluorescently stained for endoderm marker SOX17, pancreatic markers SOX9, NKX6-1 and epithelial marker ECAD. Note that SOX17 expression decreased from day 6 to day 14, whereas pancreatic marker expression increased. **B.** Representative images of confocal images at higher magnification immunofluorescently stained for PDX1 and NKX6-1 and their fluorescence intensity quantification. The number of cells analysed is denoted by n and ρ represents Spearman's rank coefficient with P-value <0.05. **C.** Representative flow cytometry quantification of PDX1/NKX6-1 double-positive cells on day 14 of EpiSC differentiation to PPs (n=2 biological experiments, see Figure S3).

144 **3D pancreatic aggregates exhibit epithelial, acinar, endocrine and endothelial markers**
145 When grown alone, PP aggregates did not grow in size over time (Fig. S4). We hypothesized that
146 inductive cues from another germ layer, most probably the mesoderm, were missing hence preventing
147 the aggregate growth. To test this hypothesis, we used EpiSC-derived mouse caudle epiblast (CE) which
148 bear characteristics of various types of mesoderm, including allantois cells and cells resembling the
149 notochord [41,42]. In the present work, this CE population was tested for its ability to recapitulate the
150 developing pancreas and its niche in the embryo. CEs, referred to here as mesoderm progenitors (MPs),
151 were mixed with PPs in a ratio that corresponded to that observed in the mouse embryo pancreas [44].
152 Each well of a 96-well plate was seeded with a 1000-cell mixture (Fig 3A), and cells aggregated to form a
153 round structure within 3 days. Culture continued for another 4 days on an orbital shaker (Fig 3B).

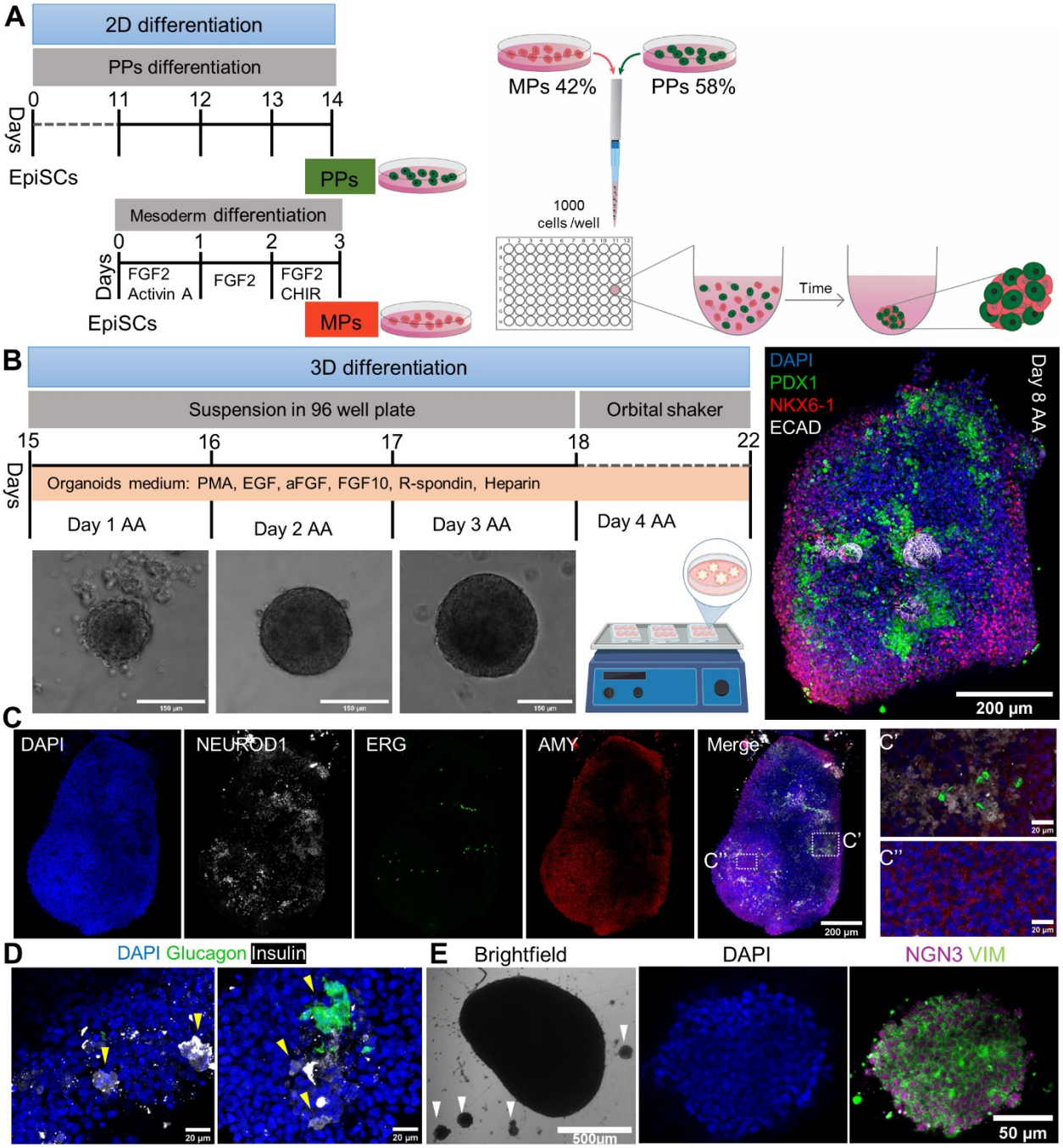

Figure 3. 3D co-culture of pancreatic and mesoderm progenitors recapitulates the developing pancreas in the embryo. A-B. A schematic illustration of pancreatic progenitor (PP) + mesoderm progenitor (MP) aggregate preparation. Prior to PP and MP aggregation, 2D differentiation courses of 14 days and 3 days were carried out to obtain PPs and MPs, respectively. **A.** On day 14, 1000 PPs and MPs were mixed at a proportion of 58% and 42% and were plated to each well of a U-bottom 96-well plate. **B.** Brightfield images of the aggregates on days 1, 2 and 3 after aggregation (AA). On day 4 AA, the aggregates were moved to a 6-well plate and placed on an orbital shaker for an additional 4 days. Confocal image of the day 8 AA aggregate immunofluorescently stained for ECAD, NKX6-1 and PDX1 (for higher magnification images see Fig. S5). **C-D.** Confocal images of day 8 AA aggregates immunofluorescently stained for endocrine marker NEUROD1, acinar marker AMY (amylase), endothelial marker ERG (C, C', C''), and glucagon and insulin, which mark alpha and beta cells, respectively (D). Nuclear staining with DAPI is in blue. Yellow arrows in D indicate regions of cells expressing insulin or glucagon. **E.** Brightfield image of a

166 pancreatic aggregate on day 8 AA. The white arrows in the image show small aggregates that are approximately
167 100-150 μm in diameter, located around the big aggregate. A representative confocal image of a small aggregate
168 immunofluorescently stained for vimentin (Vim), NGN3 and nuclei (DAPI).

169 Co-culture of PPs with MPs gave rise to pancreatic aggregates expressing various pancreas-specific
170 genes along with mesenchymal and endothelial genes. On day 8 after aggregation (AA) the PP+MP
171 aggregates expressed the pancreatic markers PDX1 and NKX6-1, contained epithelial regions marked by
172 ECAD (Fig. 3B), endocrine cells expressing NEUROD1 and NGN3 (Neurog3), regions of acinar cells
173 exhibiting AMY (amylase) expression, duct cells expressing SOX9 and weak expression of PDX1 and
174 endothelial cells marked by ERG and CD31 expression (Fig S1C and Fig. 3 and Fig. S5-S6). Furthermore, in
175 several regions in the PP+MP aggregates, endocrine cells had differentiated into beta and alpha cells
176 expressing insulin and glucagon, respectively (Fig. 3D, Fig. S6C).
177 Spatial proximity was noted between cells expressing the endothelial marker ERG and cells expressing
178 the endocrine marker NEUROD1 (Fig. S5). Specifically, cells in the outer region of the aggregate
179 expressed AMY, whilst cells deeper in the tissue expressed less AMY and more NEUROD1 and ERG. This
180 alignment between endothelial and endocrine cells (CD31 and NEUROD1 in Fig. S5, ERG and NEUROD1
181 in Fig. S6) mimics the preferential endothelial-endocrine cell organization found in the pancreas.
182 Previous studies demonstrated the importance of an endothelium for pancreas morphogenesis and
183 differentiation and for induction of endocrine differentiation in the embryo [5,45–48].
184 During the 3D culture, cells at and around the aggregate boundary had an elongated morphology, and
185 formed several small 50-100 μm aggregates, suggesting that the cells were mesenchymal with migratory
186 characteristics (Fig. 3E). Immunostaining of the small aggregates showed that most of the cells
187 expressed the epithelial-mesenchymal transition (EMT) marker vimentin (Vim) and the transient
188 endocrine marker NGN3 (Fig. 3E), similar to the profile of differentiating endocrine progenitors in the
189 embryo [49–53].

190 **Single-cell RNA sequencing analysis revealed abundant representation of mesenchymal and endocrine**
191 **populations in the PP+MP aggregates**
192 To gain a comprehensive understanding of the PP+MP aggregates and uncover the different cell
193 populations within them, the aggregates were subjected to single-cell RNA-sequencing (scRNA-seq).
194 Additionally, to assess the benefits provided by the mesodermal compartment within the pancreatic
195 aggregates, a comparative analysis was conducted at the single-cell transcriptomic level between
196 PP+MP aggregates and aggregates consisting solely of PP cells. A 3D culture of PPs mixed with Matrigel
197 was also included in the comparison, since Matrigel is commonly employed in the construction of
198 pancreatic organoids.

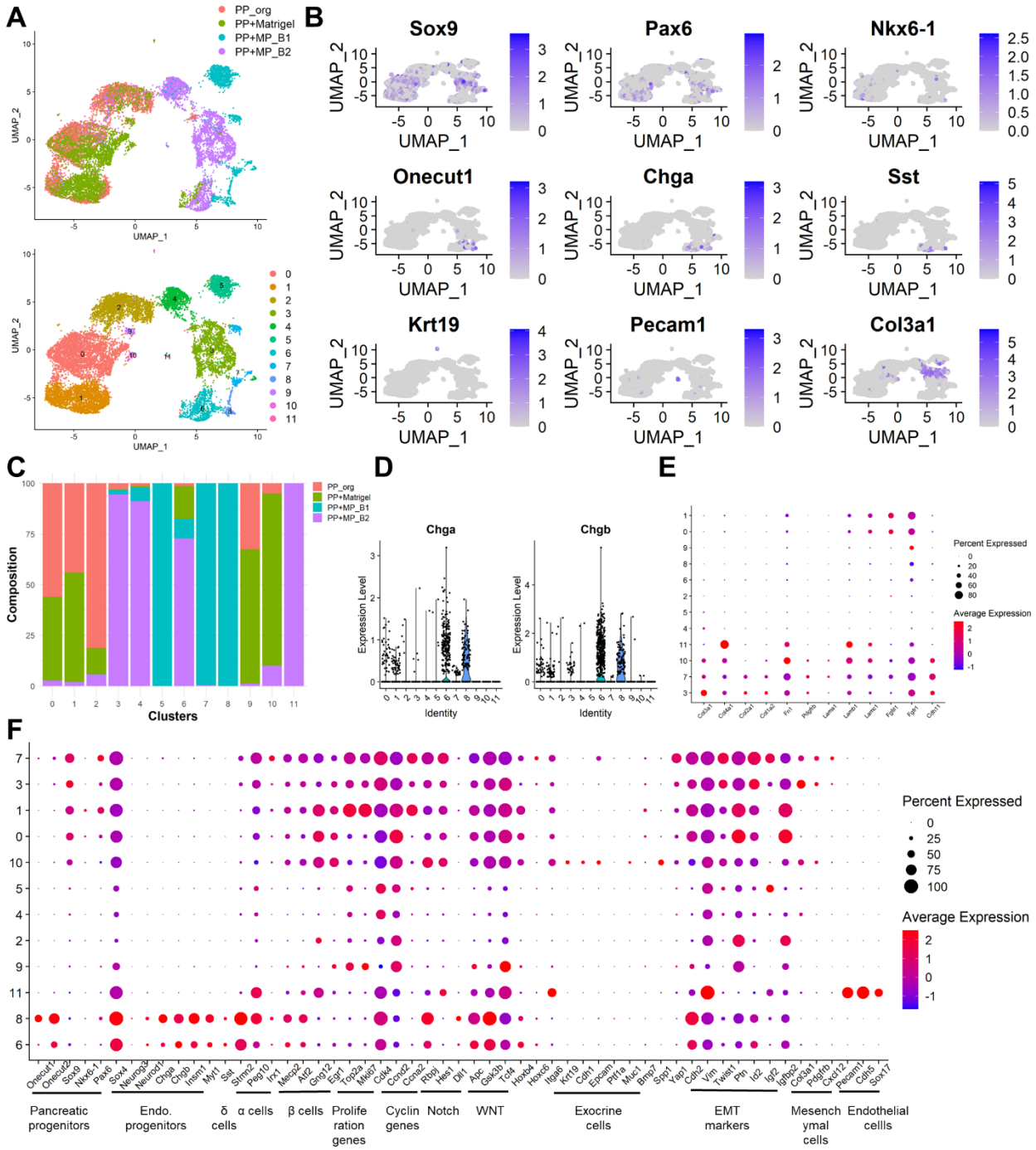

Figure 4. PP+MP aggregates show mesenchymal identity and contain endocrine populations. A. Upper graph shows dimensionality reduction UMAP plot of pancreatic aggregates coloured according to sample identity: PP aggregates (PP_org), 3D culture of PPs mixed with Matrigel (PP+Matrigel) and two biological replicates of PPs with MPs aggregates (PP+MP_B1, PP+MP_B2). At the bottom, UMAP plot of pancreatic aggregates grouped using the Seurat graph-based clustering method. The clustering algorithm (Methods) identified 12 clusters. **B.** Expression of select genes projected on the UMAP plot. Colour intensity indicates level of expression. **C.** Bar plot showing sample composition of each cluster. **D.** Violin plot visualising distribution of endocrine genes Chga and Chgb expression in each cluster. **E-F.** Expression dot plot of select genes across clusters. Clusters are ordered hierarchically based on the expression of select genes. The size of the dot corresponds to the percentage of cells expressing a gene in each cluster. The colour represents the average expression level. **E.** Expression dot plot of ECM genes, mesenchymal

genes and fibroblast growth factor receptors across clusters. **F.** Expression dot plot of select genes grouped by signalling pathway and cell identity categories (see Table S1). UMAP, uniform manifold approximation and projection. Endo. progenitors, endocrine progenitors.

Following quality control filtering (as described in the Methods section), scRNA-seq of the 3D in vitro pancreatic aggregates yielded a total of 5056 cells from the PP_org samples, 3485 cells from the PP+Matrigel samples, 1456 cells from the PP+MP_B1 samples, and 3602 cells from the PP+MP_B2 samples. A graph-based clustering algorithm revealed 12 clusters, which were visualized using the Uniform Manifold Approximation and Projection (UMAP) dimensionality reduction technique (Fig. 4A). Looking at the sample composition of the clusters (Fig. 4C) and at the genes of interest (Fig. 4B, D-F), revealed that clusters 0 and 1 were mainly comprised of PP_org and PP+Matrigel samples (Fig. 4C) and expressed laminin protein-encoding genes and FGF genes. Clusters 3 and 7, which were mainly composed of PP+MP samples, and cluster 10, which was mainly composed of PP+Matrigel cells, had mesenchymal identity and expressed ECM markers. All the clusters and predominantly clusters 0, 1, 3, 6, 7 and 8 showed EMT markers. Cluster 2, which was mainly composed of PP_org cells, and clusters 4 and 5, which were mainly composed of PP+MP samples, expressed cyclin genes. Cluster 8, which was exclusively comprised of the PP+MP samples, contained a cell population exhibiting a pancreatic progenitor signature (Onecut1, Onecut2, Pax6) and together with cluster 6, which was mainly composed of PP+MP samples, predominantly held endocrine progenitors (Sox4, Chga, Chgb, Neurod1) and included various endocrine cell types (alpha, beta and delta cells). Although some cells exhibited expression of genes found in alpha and beta cells (Fig. 4F and Table S1), expression of insulin (Ins1 and Ins2, beta cells) and glucagon (Gcg, alpha cells) was not detected in the scRNA-seq dataset. Only somatostatin (Sst, see Table S1), which is secreted by pancreatic delta cells, was detected in the dataset. Clusters 9 and 10 were mainly composed of PP+Matrigel cells and expressed proliferation genes and ductal markers (Krt19, Muc1, Cdh1 and Itga6), respectively. Cluster 11, which was exclusively composed of PP+MP samples, had endothelial identity (Pecam1 and Cdh5). Several cells across the clusters expressed exocrine progenitor markers (Ptf1a, Bmp7). Most of the cells expressed Vim (Fig. 4F), suggesting migratory and motility capacities. Many cells expressed Cdh2, also known as N-cadherin. A study that explored the expression of N-cadherin in normal human tissues suggested that N-cadherin expression is closely associated with hormone-producing cells in the pancreas but is not expressed in exocrine cells [54]. Indeed, higher expression of Cdh2 was measured in the endocrine clusters 6 and 8 and lower expression was measured in exocrine cluster 10 (Figure 4F).
In general, the PP aggregates demonstrated prominent expression of Sox9, cyclin genes, laminin genes and EMT markers. The PP+Matrigel sample primarily expressed Sox9, cyclin genes, ECM genes, EMT markers and ductal markers. The PP+MP clusters predominantly exhibited expression of EMT markers, with certain populations showing a dominant endocrine and mesenchymal identity associated with cyclin genes, similar to those observed during embryonic development ([8,55–57] and Table S1).
Focus was then placed on the pathways related to the endocrine lineage, including the expression of genes related to Notch and Wnt signaling pathways, as well as Yap1, which is part of the hippo signaling pathway. These pathways play a significant role in determining endocrine versus ductal cell lineage [58,59]. Clusters 6-8 had low expression of Notch markers and high expression of Wnt markers, suggesting their endocrine identity.
Hox gene expression profiles provide spatiotemporal information of the emerging embryonic axial tissues ([60] and reviewed in [61]). Exploring their expression in the aggregate might help anchor it to a developmental stage and region in relation to the embryo. Hoxb4 was mainly expressed in PP_org and PP+Matrigel clusters 0, 1 and 10, and PP+MP clusters 6 and 8, whereas Hoxc6 was mainly expressed in cluster 7, suggesting that cluster 7 defines a more advanced developmental stage and more posterior embryonic region as compared to the other clusters. Furthermore, Hoxb4 takes part in limiting the

257 endoderm response to signals from the notochord during the formation of the dorsal pancreatic bud [62].
258 This early stage of the pancreas might correlate with the progenitor population residing in cluster 8.
259 Hoxc6 is expressed exclusively in the mesoderm of the developing pancreas and is needed for endocrine
260 cell differentiation [62,63], suggesting a mesodermal state for cluster 7, which exclusively consisted of
261 PP+MP aggregate cells.

262 **The pancreatic aggregates captured diverse pancreatic cell types found in the mouse embryonic**
263 **pancreas**
264 To further characterize the co-culture system and evaluate its limitations, scRNA-seq data obtained from
265 the pancreatic aggregates was compared to that of mouse embryo pancreases at E12, E14 and E17 ([8]
266 and see Methods).

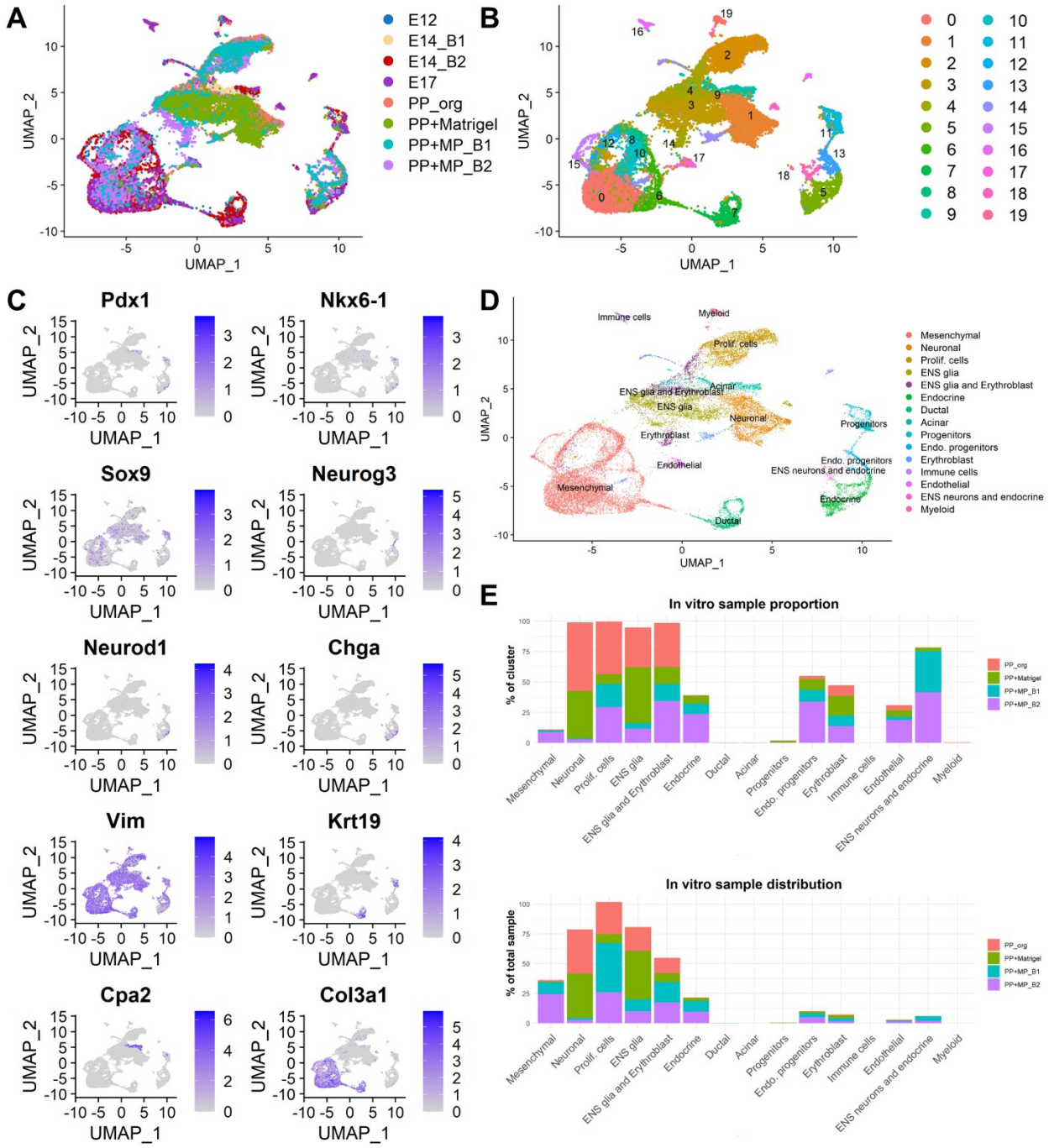

Figure 5. Comparison of single-cell RNA-seq of pancreatic aggregates and mouse embryo pancreases reveals cell population overlap. A. UMAP visualization of single-cell RNA sequencing of pancreatic aggregates: PP aggregates (PP_org, 5056 cells), 3D culture of PPs mixed with Matrigel (PP+Matrigel, 3485 cells) and two biological replicates of PPs with MPs aggregates: PP+MP_B1 (1456 cells) and PP+MP_B2 (3602 cells), and of the mouse embryonic pancreas at E12 (4412 cells), two batches at E14 (E14_B1 (3495 cells) and E14_B2 (4309 cells)) and E17 (2241 cells). Datasets were integrated using the Seurat integration algorithm. **B.** Seurat graph-based clustering revealed 20 clusters. **C.** Gene expression of select genes projected on the UMAP plot. Colour intensity indicates level of expression. **D.** A UMAP plot showing the assignment of cell type to clusters. Clusters were identified based on the expression of known markers of different pancreatic cell types as in C and as detailed in Table S2. **E.** Upper graph shows the percentage of the in vitro cells in each cell group and the bottom graph shows the distribution of the in

278 vitro cells amongst the different cell groups. Prolif. cells, proliferating cells; Endo. progenitors, endocrine
279 progenitors; ENS, enteric nervous system.

280 Integration of the 3D in vitro and embryonic datasets yielded a UMAP with 20 cell clusters (Fig. 5A-B).
281 Apart from identifying the different cell types, such as mesenchymal (Col3a1), ductal (Krt19) and acinar
282 (Cpa2) cells, the key gene expression patterns (Fig. 5C) reflected a transition from a pancreatic
283 progenitor population (cluster 11: Pdx1, Sox9 and Nkx6-1) to an endocrine progenitor population
284 (cluster 13: Neurog3), which was later committed to an endocrine lineage (cluster 5: Chga, Neurod1,
285 Ins1 and Gcg; Fig. 6C). Interestingly, high levels of Vim expression were recorded in all cell populations,
286 excluding the endocrine population, consistent with the observation that Vim is lost just after the
287 hormones are turned on during endocrine differentiation [49]. Exploring the marker gene profiles of each
288 cluster (Methods, Fig. 5C and Table S2) enabled determination of the cell identity of each cluster, which
289 is summarized on the UMAP plot in Figure 5D. A clear pancreatic identity was not assignable to cluster 2,
290 which marked by genes related to differentiating stem cells and amplifying cells, hence this cluster was
291 called proliferating cells.
292 Notably, the PP+MP aggregates displayed a distinct profile with a more abundant representation of
293 endocrine cells compared to the other in vitro samples (Fig. 5E). The PP+MP aggregates displayed a
294 diverse composition of cell types, as observed in the embryonic samples. Primarily, these aggregates
295 contained mesenchymal, endocrine and proliferating cells along with erythroblasts and enteric nervous
296 system (ENS) glia (Fig. 5E). In contrast, both PP and PP+Matrigel aggregates exhibited fewer endocrine
297 or mesenchymal cell types, with a predominant presence of neuronal and erythroblast identities.
298 Furthermore, 1.4% of the PP+MP cells were endothelial, which closely matched the proportions in the
299 E14 embryo (batch 1 with 0.92% and batch 2 with 1.04%, Table S4). In contrast, the other in vitro
300 samples demonstrated a lower endothelial cell percentage (Table S4), which suggests that inclusion of
301 mesenchymal cells in the PP+MP aggregates was important for the generation of endothelial cells
302 closely resembling the physiological proportion during pancreas development.

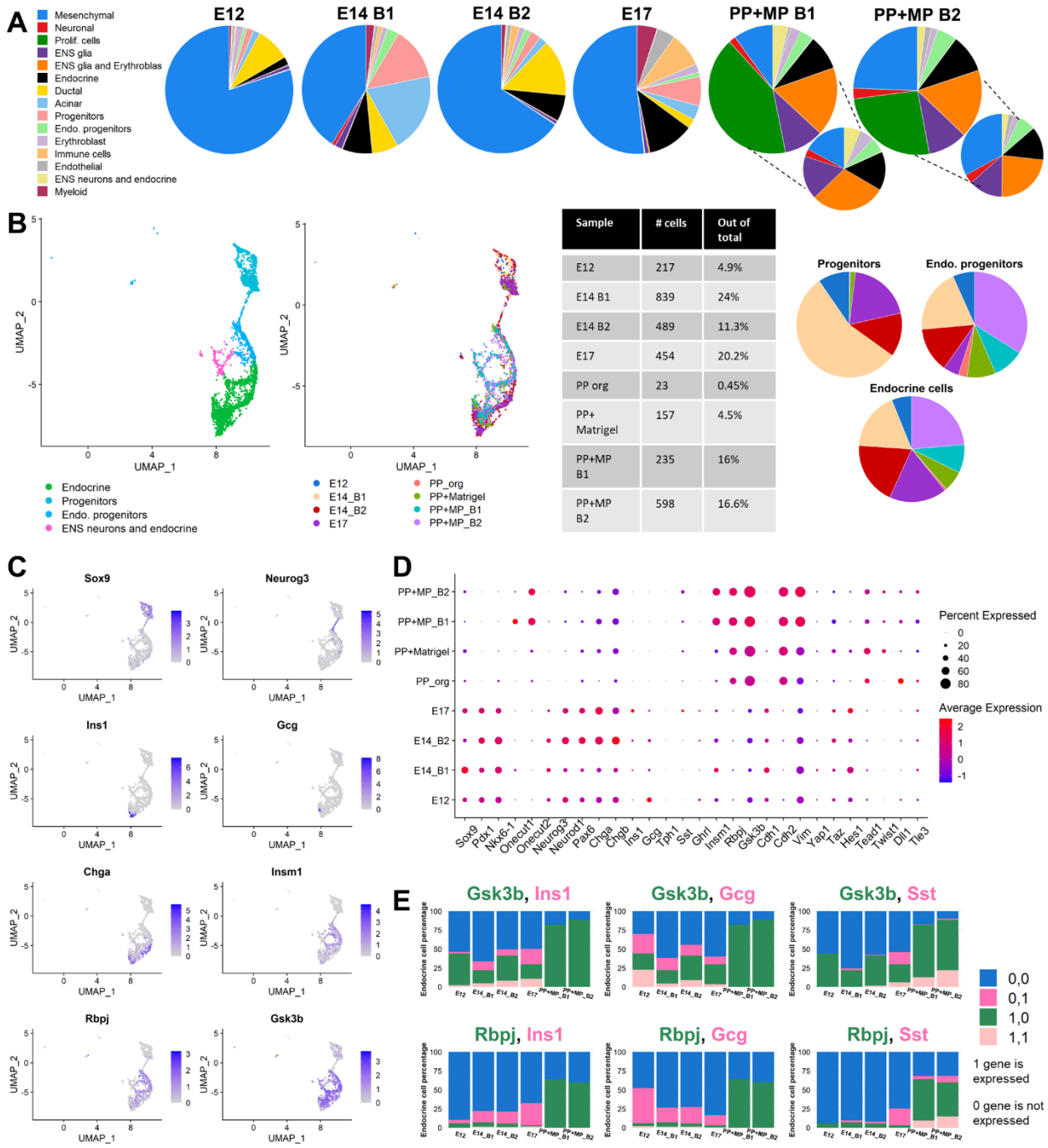

Sample	# cells	Out of total
E12	217	4.9%
E14 B1	839	24%
E14 B2	489	11.3%
E17	454	20.2%
PP org	23	0.45%
PP+ Matrigel	157	4.5%
PP+MP B1	235	16%
PP+MP B2	598	16.6%

Figure 6. Most of the in vitro to in vivo similarity is in the endocrine compartment. A. Pie plots showing the proportion of the different cell types in the mouse embryo at E12, E14 and E17 and in the 3D in vitro pancreatic samples. The lower pie plots show the proportion of the different cell types in the PP+MP samples upon exclusion of the proliferating cell cluster. **B.** UMAP of four cell types: progenitors, endocrine progenitors, endocrine and enteric nervous system (ENS) neurons and endocrine cells, coloured by cell types (left) and samples (middle). Table summarises the percentage of endocrine cells in each sample and pie plots (right) show the sample distribution in the clusters of the progenitors, endocrine progenitors and endocrine cells. The sample colour legend is presented in middle UMAP plot. **C.** Gene expression of select genes projected on the UMAP plot. Colour intensity indicates level of expression. **D.** Expression dotplot of select genes in each sample. The size of the dot corresponds to the percentage of cells expressing the gene in each sample. The colour represents the average expression level. **E.**

Composition of endocrine cells (clusters: endo. progenitors, endocrine and ENS neurons and endocrine) with double expression of either Gsk3b or Rbpj with the hormones Ins1, Gcg or Sst. 0,0 indicates neither expression of the 2 genes in a cell, 0,1 indicates no expression of Gsk3b or Rbpj and expression of the hormones (Ins1, Gcg or Sst) in a cell, 1,0 indicates expression of Gsk3b or Rbpj and no expression of the hormones (Ins1, Gcg or Sst) in a cell and 1,1 indicates expression of both genes in a cell.

In the embryonic dataset, the mesenchymal population emerged as the predominant cell population, whereas in the PP+MP aggregate samples, cluster 2, defined as a population of proliferating cells, were dominant (Fig. 6A). Neuronal and ENS glia cell types were the dominant populations within both PP aggregates and PP+Matrigel samples (Fig. S7A). Approximately 16% of the PP+MP aggregates had an endocrine identity (Fig. 6B), which is similar to the endocrine percentage in the embryonic samples at E14 (batch 1 with 24% and batch 2 with 11%) and E17 (20%, Fig. 6B). Upon exclusion of cluster 2 from the PP+MP aggregate datasets, the mesenchymal population became prominent and a significant endocrine compartment, comprising endocrine progenitors, endocrine cells and ENS neurons, was observed (Fig. 6A).

In addition to the similarity between the endocrine proportion of the PP+MP aggregates versus the in vivo system, the endocrine differentiation path was also comparable. The in vitro cells nicely projected onto the endocrine differentiation trajectory obtained in the UMAP plot (Fig.5C-D and Fig. 6B- C), from progenitors (Sox9) towards endocrine progenitors (Neurog3) and committed endocrine cells (Neurod1, Chga, Chgb). Although scRNA-seq analysis of the in vitro cells failed to detect hormones, except for Sst (Fig. 4B, F and Fig. 6D), immunostaining identified insulin and glucagon-expressing cells (Fig. 3D, Fig. S5 and Fig. S6C). Failure to detect mRNA encoding hormones in the PP+MP aggregates might have been due to their lower expression levels or to the higher expression of three genes: Rbpj, a central regulator of Notch signalling, GSk3b, a negative regulator of the Wnt pathway, and Insm1, a suppressor of Neurod1 and insulin-secreting cells (Fig. 6C-E). Almost all the cells that were positive for Ins1, Gcg or Sst in the embryonic endocrine population at different stages of pancreas development were negative for Rbpj, but some were positive for Gsk3b. Moreover, the embryonic endocrine population contained very few cells positive for Rbpj (Fig. 6E). In contrast, most of the endocrine population in the PP+MP aggregates was positive for Rbpj and Gsk3b, suggesting that Rbpj impaired full endocrine differentiation (Fig. 6E).

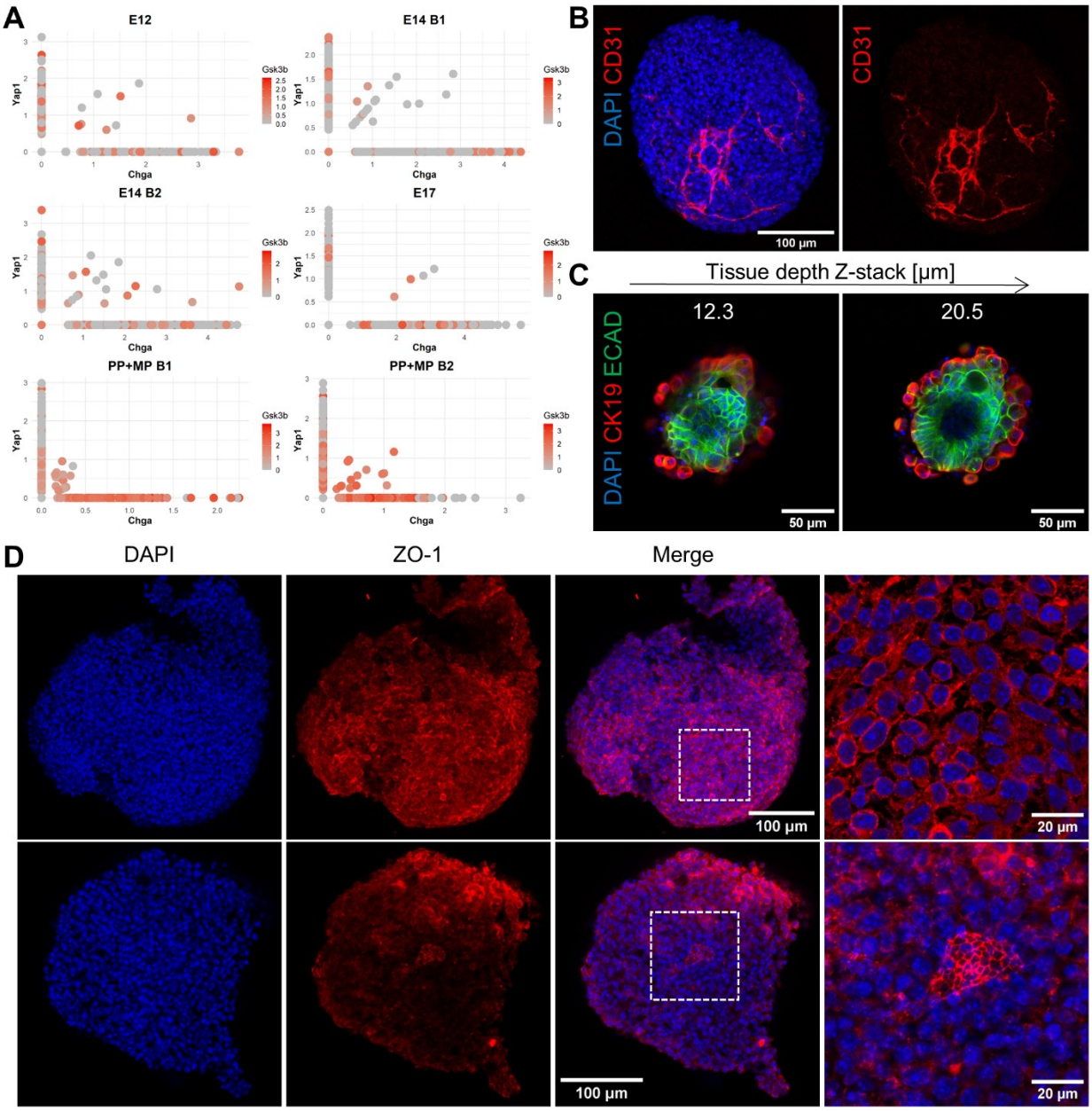

Figure 7. PP+MP aggregates do not lack mechanical cues for generating hormone-producing cells. A. Gene expression of Chga, Yap1 and Gsk3b in each sample. Each dot represents a cell, x and y axes show the normalized expression of Chga and Yap1, respectively. The normalized expression level of Gsk3b is indicated by the colour intensity. **B-C.** Confocal images of PP+MP aggregates embedded in 6.6% gelatin crosslinked with 5% microbial transglutaminase (mTG). **B.** The embedded aggregates were immunofluorescently stained for CD31, which marks the vessel-like network seen in the aggregate. **C.** The embedded aggregates were immunofluorescently stained for ECAD and CK19 (right), showing the epithelial and ductal regions at different tissue depths (Z-stacks). **D.** The non-gelatin-embedded PP+MP aggregates were immunofluorescently stained for zonula occludens-1 (ZO-1), which shows the tight junctions in the aggregates. The right-hand column presents higher-magnification images of the dashed square region in the merged image. Nuclear staining with DAPI is in blue.

To test whether the PP+MP aggregates grown in suspension have fewer alpha and beta cells in comparison to the embryo, the relation between the expression of Yap1, Chga and Gsk3b was first assessed (Fig. 7A). The absence of an outer support layer of the aggregate was thought to possibly affect

357 mechanical signalling, hence perturbing the expression of the mechanoresponsive transcription factor
358 Yap1. A recent work by Mamidi et al. [38], suggested that extracellular cues inactivate Yap1, which triggers
359 endocrinogenesis. In all samples, the Yap1 expression profile in the pancreatic aggregates is similar to
360 that found in the embryonic pancreas, with a negative relationship between Yap1 and Chga expression
361 (Fig. 7A and Fig. S7C). However, endocrine cells from the PP+MP aggregates expressed higher levels of
362 Gsk3b in comparison to those from the embryonic pancreas (Fig. 7A). The higher expression level of
363 Gsk3b might have prevented endocrine cells from further differentiating into insulin- and glucagon-
364 secreting cells.

365 To further investigate whether growing pancreatic aggregates in suspension can explain the disparity
366 between in vitro and in vivo endocrine differentiation, PP+MP aggregates were embedded in 6.7%
367 gelatin crosslinked with 5% microbial transglutaminase (mTg, Fig. 7B-C and Methods), an FDA-approved
368 enzyme that catalyses formation of covalent bonds between lysine and glutamine groups of proteins
369 and gelatin polymers [64–66]. The gelatin-mTG hydrogel was used here to provide mechanical support to
370 the aggregate, but also since it has been shown to improve cell maturation and long-term culture [64,66,67].
371 The gelatin-embedded PP+MP aggregates contained a CD31-positive vessel-like network, as well as
372 ductal regions marked by ECAD and CK19 (Fig. 7B-C and Video S1). However, insulin- and glucagon-
373 expressing cells were not detected, suggesting that mechanosignalling was not a factor limiting in vitro
374 formation of hormone-producing cells.

375 To determine whether the non-gelatin-embedded PP+MP aggregates maintained an organized epithelial
376 structure, they were immunofluorescently stained for zonula occludens-1 (ZO-1, Fig. 7D). ZO-1 staining
377 provides insights into the apical-basal polarity of tissues by visualizing tight junctions, which are crucial
378 for the establishment of barrier function and apical-basal polarity [68]. ZO-1 staining revealed intact and
379 organized tight junctions primarily localized at the apical membrane of epithelial cells within the PP+MP
380 aggregates, indicating the establishment of apical-basal polarity (Figure 7D). However ring-like epithelial
381 structures exhibiting lumen were not demonstrated, as opposed to human PSC-derived ductal
382 pancreatic organoids [17,18].

383 **Notch signalling pathway inhibition can rescue endocrine differentiation to alpha and beta cells in**
384 **PP+MP aggregates**

385 The single-cell RNA-seq analysis presented in Figure 6, which compared the endocrine populations
386 between the embryo datasets and the PP+MP aggregates, identified a difference in the expression of
387 Gsk3b and Rbpj and raised the possibility that higher expression of Rbpj in the PP+MP aggregates
388 impaired full endocrine differentiation. Therefore, the influence of inhibition of Notch and GSK3 or of
389 removal of the Wnt activator R-spondin1 on the endocrine differentiation of PP+MP aggregates was
390 assessed. The expression of progenitor, endocrine and exocrine genes of interest were compared using
391 RT-qPCR either after altering the aggregation medium throughout the 3D culture period or after
392 subjecting the aggregates to different aggregation media from day 4 AA onwards. The control was that
393 PP+MP aggregates were subjected to organoid medium without any alteration during the 3D culture
394 (Fig. 8).

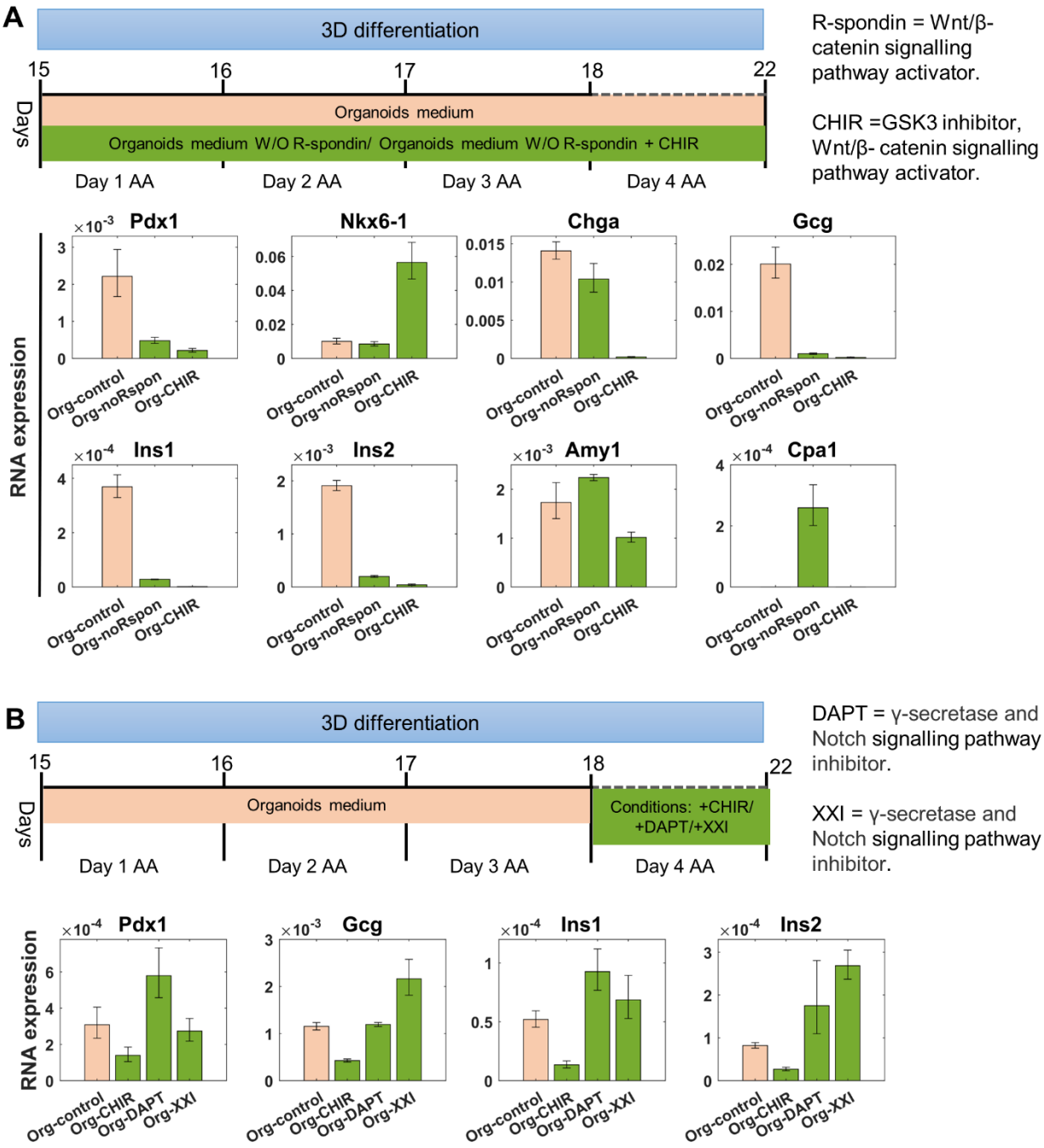

Figure 8. Inhibition of the Notch signalling pathway increased the expression of hormone-producing cells. A-B. A schematic illustration of PP+MP preparation with organoid medium alteration and RT-qPCR assessment of relative RNA expression of select pancreatic marker genes. Data are presented as averaged (n=96) aggregates per condition. Error bars indicate the SD. **A.** On day 14, 1000 mixed PPs and MPs cells were plated in each well of a U-bottom 96-well plate in organoid medium depleted from mouse R-spondin1 (Wnt activator) or in organoid medium depleted from mouse R-spondin1 and supplemented with 10 µM Chiron (GSK3 inhibitor). **B.** During the first 3 days AA, PP+MP aggregates were grown in organoid medium. From day 4 AA until the end of the differentiation, the aggregates were grown in organoid medium supplemented with either 10 µM Chiron, 1 µM DAPT (γ-secretase and Notch signalling pathway inhibitor) or 1 µM XXI (Compound E, γ-secretase and Notch signalling pathway inhibitor).

406 Removal of R-spondin1 from the aggregation medium, elevated the expression of exocrine markers
407 amylase and Cpa1 (Fig. 8A) and lowered the expression of hormone genes in comparison to the control
408 medium. Addition of CHIR, a GSK3 inhibitor, to the aggregation medium which was depleted of R-
409 spondin1, lowered the expression of both endocrine and exocrine genes, excluding Nkx6-1 (Fig. 8A).
410 Moreover, aggregates treated with CHIR seems to be larger than those grown under other conditions
411 (data not shown), suggesting that addition of CHIR increased the progenitor pool.
412 Notch inhibition was tested with DAPT or XXI, which were added to the aggregation medium from day 4
413 AA. This modification of the aggregation medium was made 4 days AA, to allow the PP+MP aggregates
414 to establish endocrine progenitors, as was indicated from the single cell RNA-seq analysis, which could
415 then, with the right signalling environment, serve as fertile ground for full endocrine differentiation.
416 Notch blocking by the two inhibitors increased the expression of Ins1 and Ins2, however only the
417 addition of XXI to the medium led to an elevation in the expression of glucagon (Fig.8B). Addition of
418 CHIR to the aggregation medium 4 days AA did not result in elevation in the hormone genes (Fig. 8B),
419 suggesting, as the single-cell RNA-seq implied, that Rbpj, a Notch activator, impaired the full endocrine
420 differentiation of the PP+MP aggregates, which was rescuable by Notch inhibition.

421 **Unique in vitro populations share similarities with the embryo**

422 The proliferating cell cluster (cluster 2) was a distinct cluster among the in vitro aggregates, which
423 scarcely contained embryonic cells (Fig. S8A). The identity of this cluster was not clear, therefore the
424 gene profile proximity between cluster 2 and other known cell types was calculated.
425 The 12 clusters found for the in vitro aggregate datasets (Fig. 4A) were projected on the aggregate-
426 embryo integrated UMAP plot (Fig. S8B). The proliferating cell cluster mainly contained cells from four in
427 vitro clusters (Fig. S8A), namely PO0, PO2, PO4, and PO5, which accounted for 99% of the proliferating
428 cell cluster and was surrounded by known embryonic clusters (Fig. S8B). To assess the similarity
429 between the four in vitro clusters in the proliferating cluster and clusters that had embryonic cells (14
430 clusters, Fig. S8), mutual information (MI) was calculated between genes and clusters. The detected
431 informative genes (Fig. S8B and Table S3) were used to calculate the cosine similarity between the 14
432 known cell types and the four in vitro clusters (Fig. S8C and methods). The in vitro clusters displayed a
433 significant similarity to erythroblast cells, with cosine similarity scores above 0.5 (similarity range was
434 between -1 to 1, whereas -1 indicates that the conditions are opposite and 1 indicates maximal
435 similarity), and to myeloid and immune cells, with approximately 0.45 cosine similarity scores (Fig. S8C).
436 Furthermore, PO0 primarily resembled neuronal cells, and also exhibited a mild similarity to pancreatic
437 progenitors, endocrine progenitors, endocrine cells and ENS neurons and endocrine (Figure S8C). PO2
438 showed similarity to neuronal cells, and mild similarity to acinar cells and ENS neurons and endocrine
439 cells. PO4 and PO5 displayed similarity to ENS neurons and endocrine cells, alongside mild similarity to
440 acinar cells, while PO5 also exhibited a mild similarity to neuronal cells. Furthermore, the cosine
441 similarity profile of the in vitro clusters corresponded to their positions in the integrated UMAP (Fig.
442 S8B). The proliferating cell cluster was surrounded by myeloid, erythroblast, immune cells and acinar
443 cells. Additionally, some cells from PO0 and PO2 were projected onto the progenitor and endocrine
444 progenitor cluster positions of the integrated UMAP (Fig. 5D and Fig. S8B). All the above suggests that
445 the in vitro clusters represent modified versions of these cell types in the in vitro environment.

446 **Discussion**

447 In this study, a well-defined in vitro culture system of mESC-derived progenitors was designed to mimic
448 development of the mouse embryonic pancreas. The first step relied on differentiation of mESCs to PPs
449 using a protocol adapted from human ESC differentiation to PPs [12]. The main changes in the
450 differentiation protocol were the removal of Matrigel and advancement of mESCs to the epiblast state

451 before differentiation. The initial pluripotency state of the cells (2i, SL and EpiSCs) prior differentiation
452 was shown to determine the capacity of the cells to differentiate to definitive endoderm and to dictate
453 the subsequent PP differentiation yield. As compared to mESCs grown in 2i and SL prior differentiation,
454 EpiSCs exhibited higher Sox17 expression at the DE stage and had a PP differentiation yield of above
455 86%, as determined by the coexpression of Pdx1 and Nkx6-1 and other pancreatic genes. This yield was
456 remarkable compared to previously reported yields of 70% or less, even after a cell sorting step [12,35–38].
457 Furthermore it emphasized the responsiveness of EpiSCs to activin and their capacity to commit to DE,
458 which is a major step in ensuring a successful PP differentiation protocol [69].
459 Two recent works made advances in achieving expandable PPs from human PSCs, either based on
460 growing expandable human PPs on feeder cell layers [70] or as PP-spheroids in Matrigel [19]. The long-term
461 maintenance and expansion of pancreatic progenitors represents a significant breakthrough in
462 biomedical research and regenerative medicine. It opens new avenues for obtaining an unlimited supply
463 of pancreatic organoids and the differentiation of these progenitors to various pancreatic cell types,
464 including beta cells. The mouse EpiSC-derived PPs described here survived a freeze-thaw cycle (data not
465 shown), however further work is still needed to establish the optimal conditions for robust PP
466 expansion. Furthermore, implementation of the recent advances in the human expandable PPs on the
467 mouse system, might shed light on the differences between human and mouse pancreatic systems.

468 After establishing a reproducible protocol for PP production, efforts were made to mimic the 3D
469 pancreatic microenvironment of the developing mouse pancreas. To this end, EpiSC-derived pancreatic
470 and mesodermal progenitors were mixed in proportions similar to those measured in the embryo [44] to
471 form an aggregate. The MPs supplied the PPs with mesodermal cues, but also cellular interactions via
472 specialized cell types, such as endothelial and mesenchymal cells, which are essential for pancreas
473 differentiation and maturation in vivo. It has been shown that growing progenitors on organ-matched
474 mesenchyme elicits their expansion and self-renewal and, importantly, gives rise to glucose-sensing and
475 insulin-secreting cells when transplanted in vivo [71]. Here, aggregation of EpiSC-derived PPs with EpiSC-
476 derived MPs without the use of Matrigel, resulted in aggregates containing a range of cell types,
477 including pancreatic progenitors, epithelial, acinar, endocrine, mesenchymal and endothelial cells.
478 Moreover, insulin and glucagon expression were detected in immunostaining analyses, indicating the
479 presence of beta and alpha cells, respectively.

480 A single-cell transcriptomic comparison between PP+MP aggregates, aggregates consisting solely of PP
481 cells and 3D culture of PPs mixed with Matrigel was then performed to gain a better understanding of
482 the benefits provided by the mesodermal compartment within the pancreatic aggregates. The scRNA-
483 seq extended the depth of the in vitro system analysis and revealed the diverse cell populations that
484 existed in the 3D in vitro systems. Notably, the PP+MP aggregates displayed a distinct profile with a
485 more abundant representation of endocrine cells compared to PP and PP+Matrigel aggregates.
486 Moreover, PP+MP aggregates demonstrated higher endothelial cell percentage in comparison to the
487 other in vitro samples. These finding suggests that endothelial cells are important for endocrine
488 differentiation, as indicated by previous studies which showed that endothelial cells repress acinar
489 differentiation whilst increasing endocrine differentiation [48,72].
490 The cell population comparison between the three in vitro systems further indicated that although
491 PP+MP aggregates showed no deficiency in ECM proteins, the addition of Matrigel to PPs induced the
492 expression of ductal markers. Recent studies showed that Matrigel triggered epithelial morphogenesis in
493 vitro, as demonstrated, for example, by the emergence of a neural tube shape after embedding
494 aggregates of mouse ESCs in Matrigel [73], epithelia dome-shaped structures of human PSC monolayers
495 grown in the presence of Matrigel in [74] and epithelial ring organization with apical-basal cell polarity of
496 human PSC-derived ductal pancreatic organoids cultured with Matrigel [17,18]. In the present study, the

497 hydrogel-free PP+MP aggregates expressed the tight junction marker ZO-1 but did not exhibit lumen- or
498 ring-like structures similar to those observed in the ductal pancreatic organoids. In contrast, the gelatin-
499 embedded PP+MP aggregates showed improvement in the epithelial organization, suggesting that
500 gelatin, by imposing biophysical constraints, together with the mesodermal compartment, providing
501 biochemical signals, can compensate for the Matrigel epithelial patterning regulation. Overall, the
502 discrepancy in cell type composition between the in vitro systems highlights the unique characteristics
503 and potential of PP+MP aggregates.

504 Some discrepancies were found between the immunofluorescence staining and the scRNA-seq results,
505 mainly related to insulin and glucagon, which were not detected at the mRNA level. This may have been
506 due to the pooling of single cells from hundreds of aggregates for the scRNA-seq analysis, which might
507 have interfered with the detection of rare cell types and genes expressed at low levels, e.g., hormone-
508 secreting cells.

509 The comparison of single-cell transcriptomes of the 3D in vitro samples to the embryonic data collected
510 at E12, E14 and E17 demonstrated that the in vitro aggregates succeeded in recapitulating many of the
511 cell populations residing in the pancreas. Remarkably the PP+MP aggregates had an endocrine
512 compartment similar in its size to that of the E14 and E17 pancreas and endothelial compartment similar
513 to that of the E14 pancreas. On the other hand, the PP and PP+Matrigel samples exhibited dominant
514 neuronal populations. Resemblance to the embryonic pancreas was not only in the relative size of the
515 endocrine population but also in the differentiation path from the progenitors to endocrine cells,
516 particularly in the PP+MP sample. Yet the PP+MP aggregates did not entirely mirror the embryo and
517 contained a population (cluster 2) that was distinct from the embryonic pancreatic cells. Although this
518 population was mainly composed of in vitro cells that did not cluster with the embryonic pancreatic
519 cells, they exhibited a gene profile that was close to known clusters as erythroblast, myeloid,
520 progenitors and endocrine cells. This gene profile discrepancy between the pancreatic aggregate cells
521 and the in vivo cells, might reflect differences in the main signalling pathways driving pancreas
522 development, i.e., Notch, Wnt and Hippo pathways. A recent work by Mamidi et al. [38], suggested that
523 extracellular cues inactivating Yap1 trigger endocrinogenesis. In the current in vitro system, although the
524 PP+MP aggregates were grown in suspension and lacked the mechanical support typically provided by
525 Matrigel, most of the cells that were positive for Chga were also negative for Yap1, indicating that the in
526 vitro progenitors can produce endocrine cells. The endocrine cells of the PP+MP aggregates also
527 expressed higher level of Gsk3b, a Wnt repressor, and of Rbpj, a central regulator of Notch signalling, in
528 comparison to the embryo. Notch signalling helps maintain progenitor proliferation and prevents
529 premature differentiation to ductal and endocrine fate [58,75]. Wnt signalling regulates pancreatic
530 specification and patterning during different stages of pancreas development [58,59]. On the one hand,
531 Wnt inhibition is necessary for endocrine differentiation [76], but, on the other hand, deletion of Wnt-
532 related genes has been found to reduce the proportion of pancreatic progenitors, which subsequently
533 reduces the number of both endocrine and exocrine cells [58]. In light of an earlier report that Gsk3b
534 overactivation results in decreased pancreatic beta cell proliferation and mass [77] and that high levels of
535 Notch signalling lead to the repression of Neurog3, preventing endocrine cell fate determination [58], the
536 ability of Gsk3b and mainly Rbpj to limit endocrine cells from further differentiating into insulin- and
537 glucagon-secreting cells was evaluated here. Exposure of PP+MP aggregates to Notch inhibitors
538 increased the expression of insulin and glucagon, however addition of GSK3 inhibitor to the aggregate
539 growth medium did not increase the expression of hormone genes, indicating that indeed Rbpj impaired
540 full endocrine differentiation in the PP+MP aggregates. Overall, the transcriptomic analyses revealed the
541 similarities and differences between the pancreatic aggregates and the mouse embryonic pancreas and

542 highlighted signalling pathways and mechanisms that may govern pancreas progenitor differentiation
543 and development.
544 To further determine whether the lack of mechanical cues generally provided by Matrigel, prevented
545 the emergence of insulin- and glucagon-producing cells in the in vitro system, the PP+MP aggregates
546 were embedded in a gelatin-mTG hydrogel, which constrains cells in space. However, cells positive for
547 insulin or glucagon were not detected in the gelatin-embedded aggregates, implying that mechanical
548 cues are either already present via the MP counterpart of the aggregate or that they are not the key
549 determinant of full endocrine differentiation in this pancreatic in vitro model. Nevertheless, the gelatin-
550 embedded aggregates were highly vascularized and displayed epithelial ductal regions, which are
551 important for in vitro maturation and indicate correct development. Achieving such vascularization is an
552 advancement in tissue engineering, since vascularization is important for growth, prevents necrosis as
553 the aggregates increase in size and prevents premature differentiation [78].

554 Until recently, the study of embryo and organ development has been restricted to animal embryos and
555 fetal tissues. Although organogenesis can be observed in the embryo, these animal models and material
556 sources are limited, and their use presents ethical concerns. The increasing utilization of human and
557 mouse stem cell-derived organoids has significantly expanded the study of mammalian development
558 and promoted regenerative and therapeutic medicine, whilst reducing the use of animals. Nevertheless,
559 most organoids, and specifically pancreatic organoids, rely on the use of Matrigel, which limits
560 reproducibility and full definition of an in vitro 3D system. The present study aimed to maximize in vitro
561 resources to construct a new in vitro system by mixing endoderm- and mesoderm-derived progenitors in
562 a defined proportion. In the future, these mixtures can be explored in the in vitro system, and might
563 shed light on the important interactions between the endoderm- and mesoderm-derived progenitors.
564 The novel system closely recapitulated key elements of mouse embryonic pancreas and bears the
565 potential to serve as a tuneable model for the study of mammalian pancreas development and pancreas
566 diseases.

567 **Methods**

568 **Cell culture**

569 ES-E14TG2a (ATCC CRL-1821) mouse embryonic stem cells were grown in sterile flasks pre-coated with
570 0.1% porcine skin Type A gelatin (Sigma-Aldrich, G1890) in pluripotency medium referred to as serum
571 and LIF (SL), comprised of GMEM (Gibco) supplemented with 1% non-essential amino acids (100X
572 Gibco), 1 mM sodium pyruvate (Biological Industries), 1% GlutaMAX (100X Gibco), 0.1 mM β-
573 mercaptoethanol (Gibco), 10% foetal bovine serum (FBS) (HyClone, Thermo Fisher Scientific), and 10
574 ng/ml LIF (R&D Systems). Cells were maintained at 37 °C in 5% CO_2. Medium was changed daily, and
575 cells were passaged with trypsin (Biological Industries) every 2-3 days, as necessary, up to a total of 30
576 passages.

577 **2i**

578 2i was comprised of basal differentiation medium NDiff®227 (Takara), hereby referred to as N2B27,
579 supplemented with 1 µM MAPK inhibitor PD0325901 (Sigma-Aldrich, referred as PDO3) and 3 µM GSK3β
580 inhibitor CHIR99021 (Sigma-Aldrich, referred to as Chiron). Cells grown in 2i medium are in a stringent
581 pluripotency environment and are considered to be at ground-state pluripotency [32].

582 **Epiblast stem cell and Epi-medium**

583 ES-E14TG2a were grown in plastic tissue-culture flasks coated with 5 µg/ml plasma fibronectin (F0895, 1
584 mg/ml, Sigma-Aldrich) in Dulbecco's phosphate-buffered saline (DPBS with calcium and magnesium,
585 Sigma-Aldrich, D8662). mESCs were grown in Epi-medium which was comprised of N2B27 supplemented

586 with 12 ng/ml FGF2 (Peprotech) and 25 ng/ml Activin A (Peprotech), for at least four passages, to
587 generate EpiSCs [42].

588 **Differentiation of mESCs to pancreatic progenitors (PPs)**
589 The differentiation protocol below is a variation of one previously used to derive PPs from human
590 pluripotent stem cells [12]. Prior to differentiation, mESCs were grown in either SL or 2i or as EpiSCs in Epi-
591 medium. Cells grown in SL and 2i were grown in sterile flasks pre-coated with 0.1% gelatin, whereas
592 flasks with EpiSCs were pre-coated with 5 µg/ml fibronectin.
593 Cells were plated at a density of $5x10^4$ cells/cm^2 in their respective growth medium (SL, 2i or Epi-
594 medium) 24 h prior to differentiation (day 0). The backbone medium for the first 5 days of
595 differentiation was BE1: MCDB131 (Gibco) supplemented with 0.8 g/L cell-culture-tested glucose
596 (Sigma-Aldrich), 1.174 g/L sodium bicarbonate (Biological Industries), 0.1% fatty acid-free (FAF) bovine
597 serum albumin (BSA) (Sigma-Aldrich) and 2 mM GlutaMAX. The backbone medium for the subsequent 9
598 days of differentiation was BE3: MCDB131 supplemented with 0.44 g/L glucose, 1.754 g/L sodium
599 bicarbonate, 2% FAF-BSA, 2mM GlutaMAX, 4.4 mg/L-ascorbic acid (Sigma-Aldrich) and 0.5x insulin-
600 transferrin-selenium-ethanolamine (Gibco). Cells undergoing differentiation were cultured at 37 °C in a
601 5% CO_2 incubator and medium was changed daily. On day 1, cells were washed with DPBS and incubated
602 with BE1 supplemented with 3 µM Chiron (CHIR99021, Sigma-Aldrich) and 100 ng/mL activin A. On day
603 2, medium was replaced by BE1 with 100 ng/mL activin A for 2 days. On day 4, medium was changed to
604 BE1 with 50 ng/mL keratinocyte growth factor (KGF also known as FGF7, Peprotech) for 2 days. On days
605 6-9, cells were cultured in BE3 medium containing 0.25 µM SANT-1 (Sigma-Aldrich), 2 µM retinoic acid
606 (Sigma-Aldrich), 200 nM LDN-193189 (Sigma-Aldrich) and 500 nM PDO3 (PD0325901 Sigma-Aldrich). On
607 days 10–14, the cells were cultured in BE3 supplemented with 50 ng/mL FGF10 (R&D systems), 330 nM
608 Indolactam V (Cayman), 10 µM SB431542 (Tocris) and an additional 16 mM glucose. An outline of the
609 differentiation protocol is presented in Fig. 1A.

610 **Mesoderm progenitors (MPs)**
611 The protocol for differentiation of EpiSCs to mouse embryo caudle epiblast (CE)-like cells is detailed in
612 [41,42]. Briefly, EpiSCs were differentiated to Epi-CE, which resemble the caudle epiblast of the mouse
613 embryo and contain the different mesoderm compartments: lateral plate mesoderm, intermediate and
614 paraxial mesoderm, hence we refer to these cells here as mesoderm progenitors. EpiSCs were plated at
615 a density of 5×10^4 cells/cm^2 in a flask pre-coated with 5 µg/ml fibronectin and grown in Epi-medium for
616 the first day (day 0). On Day 1, medium was replaced with N2B27 supplemented with 20 ng/ml FGF2 and
617 without activin A. On day 2, N2B27 was supplemented with 3 µM Chiron and 20 ng/ml-FGF2.

618 **Aggregate preparation**
619 <u>PP+MP aggregates</u>
620 PPs and MPs in adherent culture were dissociated from culture flasks with accutase (STEMCELL
621 Technologies) on days 14 and 3 of differentiation, respectively. Cells (n=1000) at a ratio of 58% PPs and
622 42% MPs were plated in each well of a U-bottom 96-well plate in 50 µL organoid medium comprised of
623 Dulbecco's Modified Eagle Medium/Nutrient Mixture F-12 (DMEM/F-12(HAM)1:1, Biological Industries)
624 with 10% knockout serum replacement (KSR, Gibco), 1% penicillin-streptomycin (PS, Biological
625 Industries), 0.1 mM β-mercaptoethanol (Gibco), 16 nM phorbol myristate acetate (PMA, Sigma-Aldrich),
626 5 µM ROCK inhibitor (Thazovivin, Sigma-Aldrich), 25 ng/mL epidermal growth factor (EGF, Sigma-
627 Aldrich), 500 ng/ml mouse R-spondin1 (R&D systems), 2.5 U/mL heparin sodium salt (Sigma-Aldrich), 25
628 µg/mL acidic fibroblast growth factor (aFGF, R&D systems) and 100 ng/mL FGF-10 [23]. After 48 h, 100 µL
629 of the same medium was added to each well for an additional 48 h. On day 4 AA, the aggregates were
630 transferred to a 6-well plate and placed on an orbital shaker operating at 110 RPM (RCF of 0.11808g and

631 shaking diameter of 10mm) for an additional 4 days (total 22 days of differentiation, Fig. 3B). Wells were
632 supplemented with 3 ml organoid medium, of which 1 ml was changed every 2 days from day 4 AA until
633 the end of differentiation.
634 Aggregate cell ratio justification: At embryonic stages E12.5 and E14.5, the pancreas was composed of
635 58% epithelial cells, 37% mesenchymal cells and 5% endothelial cells (Fig. 5C in [44]). The mesoderm gives
636 rise to mesenchyme, endothelium and blood cells [4,79], hence MPs represent the mesenchymal and
637 endothelial cells and PPs represent the epithelial compartment of the pancreas embryo, requiring in a
638 ratio of 58% PPs and 42% MPs in an aggregate (Fig. 3A).
639 PP aggregates
640 PPs in adherent culture were dissociated from culture flasks with accutase on day 14 of differentiation.
641 1000 cells were plated in in each well of a U-bottom 96-well plate in 50 µL organoid medium. Culture
642 and medium change were the same as for PP+MP aggregates.
643 PP+Matrigel
644 Generation of PP aggregates in Matrigel was based on a protocol previously described for human PP-
645 spheroids [19]. PPs in adherent culture were dissociated from culture flasks with accutase on day 14 of
646 differentiation. One part of $4x10^6$ cells/ml was mixed with 3 parts of Matrigel (Matrigel® Growth Factor
647 Reduced (GFR) Basement Membrane Matrix, Phenol Red-free, LDEV-free, Corning® 356231). An example
648 for cells-Matrigel mixture volumes is 40 µl of $4x10^6$ cells/ml mixed with 120 µl Matrigel. Drops of 40 µl
649 cells-Matrigel mixture (40,000 cells per drop) were slowly dispensed onto the center of each well of pre-
650 warmed 4-well plates (Nunc cell culture, Thermo Fisher Scientific), to form a 3D dome. The plates were
651 incubated at 37 °C for 10 min to allow the Matrigel to solidify and then 500 µl organoid medium was
652 added to each well. Organoid medium was changed every 3 days.

653 **RNA extraction and real-time quantitative polymerase chain reaction (RT-qPCR)**
654 RNA was extracted at different time points during EpiSC differentiation to PPs using the RNeasy
655 extraction kit (Qiagen), according to the manufacturer's instructions. RNA concentration was measured
656 with a NanoDrop (NanoDrop One, Thermo Fisher Scientific). cDNA was synthetized using the high-
657 capacity cDNA Reverse Transcription Kit (Applied Biosystems, Thermo Fisher Scientific), according to the
658 manufacturer's instructions. RT-qPCR was performed using Fast SYBR Green Master Mix (Applied
659 Biosystems, Thermo Fisher Scientific), according to the manufacturer's instructions. The gene-specific
660 primers that were used are listed in Table 1. The reaction was performed in a QuantStudio1 (Applied
661 Biosystems, Thermo Fisher Scientific), in technical triplicates. All experiments were performed in
662 biological triplicates. Expression values were normalized against the housekeeping gene Ppia ($2^{-\Delta ct}$). The
663 results are presented as the average across biological replicates ($2^{-mean(\Delta ct)}$) with the standard error of
664 the mean (SEM, $2^{-(mean(\Delta ct)\pm sem(\Delta ct))}$).

665 **Table 1**. qPCR primer list

Gene	Forward primer	Reverse primer
Ppia	TTACCCATCAAACCATTCCTTCTG	AACCCAAAGAACTTCAGTGAGAGC
Nanog	CCTCCAGCAGATGCAAGAA	GCTTGCACTTCATCCTTTGG
Sox2	CATGAGAGCAAGTACTGGCAAG	CCAACGATATCAACCTGCATGG
Oct4	CCAATCAGCTTGGGCTAGAG	CTGGGAAAGGTGTCCCTGTA
Fgf5	TGGCATTATGTGGAATCTGG	CTGTGGACGCTGCACACTT
Sox17	GTAAAGGTGAAAGGCGAGGTG	GTCAACGCCTTCCAAGACTTG
Foxa2	CATTACGCCTTCAACCACCC	GGTAGTGCATGACCTGTTCG
Ecad	CAATGCCTGCTCTTGATGGT	GGGAGATCTGACTGCCTCTG
Pdx1	CATCGCGCCACTGCGAC	TTTCTTCTTGTGCGACGCC
Nkx6-1	AACACACCAGACCCACGTTC	GAACCAGACCTTGACCTGACTC
Sox9	AGACTCACATCTCTCCTAATGCT	ACGTCGGTTTTGGGAGTGG

Ptf1a	AGGTTATCATCTGCCATCGAG	GACACAAACTCAAAGGGTGGT
Pax6	AAGCACTTCACTTTGTAACTGTCC	CCAACTGATACCGTGCCTTC
Insm1	GCCCAGGTGTTCCCCTGCAA	AGGCCCGGGGAGCTGTAGAA
Chga	CAAGTTTTTGCCCTTCCTGT	CAGCGAGTCGGAGATGACTT
Ins1	GCAAGCAGGTCATTGTTTCAAC	AAGCCTGGGTGGGTTTGG
Ins2	ACCCACAAGTGGCACAACTG	TACAATGCCACGCTTCTGC
Gcg	GCACATTCACCAGCGACTACA	CGGTTCCTCTTGGTGTTCATC
Amy1	GCTGCTCAGGTCAGAGATTGT	CTGAACCCTGCTACGCCAAT
Cpa1	GTCTTGGTCTCAGCCTGACC	CCGCCAGAAGTCCAACTTCAA

Cell viability assay

The 3-(4,5-dimethylthiazol-2-yl)-2,5-diphenyltetrazolium (MTT) assay based on the conversion of MTT to blue formazan crystals by viable cells, was used to measure cell viability. Briefly, 24 h after mESCs were grown in either 2i, SL or as EpiSCs in Epi-medium (day 0) and on days 4, 6 and 10 during PP differentiation, the medium was removed and replaced with a fresh MCDB131 medium with 0.5 mg/ml MTT (Glentham Life Sciences, GC4568 Corsham, UK). After incubation at 37 °C for 2 h, the medium was discarded and 100 µl DMSO was added to each well. The plate was incubated at room temperature for an additional 2 h and absorption was determined in a microplate reader (Synergy H1, BioTek) at λ = 570 nm/650 nm after automatic subtraction of background readings. Cell viability was expressed as the percentage of total EpiSCs at the relevant time point during PP differentiation.

Immunofluorescence and confocal imaging

Cells and aggregates were washed with phosphate-buffered saline (PBS) 1X (Gibco) and fixed in 4% paraformaldehyde (PFA) (ChemCruz, Santa Cruz Biotechnology) for 15 min at room temperature (RT). Samples were washed and permeabilized for 15 min with PBST:PBS 1X + 1mM $CaCl_2$, supplemented with 0.5% bovine serum albumin (BSA) (Millipore) and 0.5% Triton X-100 (Bio-Lab Ltd.) before overnight incubation at 4 °C with primary antibodies diluted in PBST. Antibody used are listed in Table 2. The following day, samples were washed with PBST and incubated at room temperature for 2 h with secondary antibodies and 4',6-diamidino-2-phenylindole (DAPI) (Sigma-Aldrich) diluted in PBST. Samples were washed with PBS 1X and stored in fresh PBS 1X at 4 °C until imaging. Aggregates were mounted on microscope slides by pipetting them in 15 µl droplets of Fluoromount-G (SouthernBiotech, 0100-01) and then covered with a microscope cover glass (No. 1.5H 24 mm x 60 mm) with an adhesive spacer (Silicone isolators, press-to-seal, Sigma-Aldrich). Cells and aggregates were imaged using a confocal microscope (LSM700, Ziess) and Fiji software (ImageJ) was used to process and analyse the images.

Table 2. Primary and secondary antibodies used for immunofluorescence staining of cells and aggregates

Antibody	Dilution	Manufacturer	RRID
Rabbit anti-PDX1	1:2200	ab47267 Abcam	AB_777179
Guinea pig anti-PDX1	1:500	ab47308 Abcam	AB_777178
Mouse anti-NKX6-1	1:400	F55A12-c DSHB	AB_532379
Mouse anti-Sox9	1:500	SC-166505 Santa Cruz	AB_2255399
Goat anti-Sox17	1:200	AF1924 R&D	AB_355060
Rat anti-Ecad	1:200	U3254 Sigma-Aldrich	AB_477600
Mouse anti-neurogenin3 (C-7)	1:500	SC-374442 Santa Cruz	AB_10988579
Mouse anti-amylase	1:200	SC-46657 Santa Cruz	AB_626668
Rabbit anti-ERG	1:500	ab92513 Abcam	AB_2630401
Mouse anti-glucagon	1:1000	G2654 Sigma-Aldrich	AB_259852
Guinea pig anti-insulin	1:200	A0564 DAKO	AB_10013624

Goat anti-neuroD1	1:300	AF2746 R&D	AB_2149217
Rabbit anti-cytokeretin19 (CK19)	1:500	ab133496 Abcam	AB_11155282
Rabbit anti-Cdx2	1:500	ab76541 Abcam	AB_1523334
Rabbit anti-Tbx3	1:100	ab99302 Abcam	AB_10861059
Rabbit anti-vimentin	1:1000	ab92547 Abcam	AB_10562134
Rat anti-CD31	1:50	550274 BD Biosciences	AB_393571
Rabbit anti-ZO-1	1:100	21773-1-AP Proteintech	AB_10733242
Donkey anti-rat Alexa fluor 488	1:400	A48269 ThermoFisher Scientific	AB_2893137
Donkey anti-guinea pig Alexa fluor 488	1:200	706-545-148 Jackson Immunoresearch Laboratory	AB_2340472
Donkey anti-goat Alexa fluor 488	1:400	A32814 ThermoFisher Scientific	AB_2762838
donkey anti-mouse Alexa fluor 488	1:400	A32766 ThermoFisher Scientific	AB_2762823
Donkey anti-guinea pig Alexa fluor Cy3	1:500	706-165-148 Jackson Immunoresearch Laboratory	AB_2340460
Donkey anti-mouse Cy3	1:400	715-165-150 Jackson Immunoresearch Laboratory	AB_2340813
Donkey anti-rabbit Cy3	1:400	711-165-152 Jackson Immunoresearch Laboratory	AB_2307443
Goat anti-rat Alexa fluor 647	1:400	A48265 ThermoFisher Scientific	AB_2895299
Donkey anti-rabbit Alexa fluor 647	1:400	A32795 ThermoFisher Scientific	AB_2762835
Donkey anti-mouse Alexa fluor 647	1:100	715-605-150 Jackson Immunoresearch Laboratory	AB_2340862
Donkey anti-rat Cy5	1:200	712-175-150 Jackson Immunoresearch Laboratory	AB_2340671

690 **Flow cytometry**
691 To assess the differentiation of EpiSCs to PPS, flow cytometry was performed on day 14 using mouse
692 anti-NKX6-1 and rabbit anti-PDX1 antibodies (Table 2). EpiSC-derived PPs were fixed in 4% PFA for 15
693 min. Cells were centrifuged at RT for 3 min at 300 *g* to remove the fixation solution, and then washed in
694 PBST. The cells were incubated with anti-PDX1 and anti-NKX6-1 primary antibodies overnight at 4 °C.
695 The following day, the cells were centrifuged at RT for 5 min at 300g, washed in PBST and centrifuged at
696 RT for 5 min at 300g. Next, the cells were incubated with donkey anti-mouse Alexa fluor 647 (1:100,
697 Jackson Immunoresearch Laboratory) and donkey anti-rabbit Cy3 (1:400, Jackson Immunoresearch
698 Laboratory) secondary antibodies for 2 h at RT, in the dark. Cells were washed in PBST, centrifuged at RT
699 for 5 min at 300g and resuspended in PBS 1X. Control samples were incubated with secondary
700 antibodies only. Cells were analysed using the BD FACS Aria-IIIu cell sorter (BD) and the data were
701 analysed with FlowJo analysis software (BD).

702 **Single-cell RNA sequencing (scRNA-seq)**
703 On day 22 (day 8 AA), PP+MP aggregates (2 biological replicates), PP aggregates and PP+Matrigel were
704 dissociated into single cells. PP+MP and PP aggregates were dissociated with accutase, whereas
705 PP+Matrigel were dissociated with TrypLE Select 1X (Gibco). A 10x Genomics single-cell transcriptomic
706 service was used to sequence the cells of the aggregates. For batch 1, a single-cell RNA sequencing
707 library was generated for 3,121 cells from PP+MP aggregates, while for batch 2, three libraries were

708 generated for 6,602 cells of PP+MP aggregates, 7,575 cells of the PP aggregate and 4,240 cells of the
709 PP+Matrigel sample. Briefly, after applying various filtering steps, a total of 1456 and 3602 cells of
710 PP+MP aggregates from batch 1 and batch 2 respectively, 5,056 cells of PP aggregate and 3,485 cells of
711 PP+Matrigel were retained for subsequent analysis. To group cells by cell types, the graph-based
712 clustering R package Seurat v4.3.0 [80] and the batch correction R package Canek version 0.2.1 [81] was
713 used, followed by visualization using Uniform Manifold Approximation and Projection (UMAP)
714 dimensionality reduction technique.

715 *Library preparation and data generation*
716 One RNA single-cell library for batch 1 and 3 RNA single cell libraries for batch 2 were prepared at the
717 Technion Genomics Centre, according to the 10x manufacturer's protocol (Chromium Next GEM Single
718 Cell 3' Library & Gel Bead Kit v3.1, PN-1000121), using 7,000 and 15,000 input cells per sample for batch
719 1 and batch 2, respectively. Single-cell separation was performed using the Chromium Next GEM Chip G
720 Single Cell Kit (PN-1000120). The RNA-seq data was generated on Illumina NextSeq2000, P2 100 cycles
721 (Read1-28; Read2-90; Index1-10; Index2-10) (Illumina, cat no. 20046811). Cell Ranger version 6 and
722 version 7.1 (for batch 1 and batch 2 respectively, 10x Genomics) was used to process raw sequencing
723 data and the Seurat R package version 4.3.0 [80] was used to build the expression matrix. Gene expression
724 was quantified by unique molecular identifiers (UMI) counts.

725 *Mouse embryo single-cell RNA-seq data*
726 The single-cell transcriptomic data of pancreatic aggregates was compared to transcriptomic data of the
727 mouse pancreas collected on embryonic days 12, 14, and 17 [8]. As detailed by Byrnes et al. [8], single-cell
728 RNA-sequencing libraries were generated for 4,631 cells on E12, 9,028 cells on E14 (comprised of two
729 independent batches E14_B1 and E14_B2), and 4,635 cells on E17. Cell and gene filtering, normalization
730 and data integration between the in vitro and the embryo samples were all performed with R package
731 Seurat version 4.3.0 [80].

732 *Single-cell data clean up and quality control*
733 Using Seurat R package version 4.3.0 [80], the expression matrix was cleaned as follows: 1) UMI counts:
734 only cells that had 500-70,000 UMI counts were retained for further analysis, ensuring a sufficient
735 sequencing depth for each cell. 2) Detected genes: only cells that had 500-8000 unique genes in a cell
736 were retained for further analysis, to ensure that the reads were distributed across the transcriptome.
737 3) Mitochondrial gene expression: an upper limit of 20% mitochondrial genes (mitochondrial gene
738 counts in a cell versus the total detected genes in a cell) in a cell was set, to reduce the likelihood that
739 cells for further analysis were dead or stressed. 4) Gene filtering: a threshold of at least 5 cells
740 containing more than 1 UMI of a gene was set. The number of cells and total genes after the clean-up
741 are presented in Table 3. The aggregate data was processed with Seurat version 4.3.0 and batch
742 correction was performed with Canek R package version 0.2.1 [81]. First, the expression matrix was log-
743 normalized and then scaled (linear transformed), such that the mean and the variance expression of
744 each gene across cells was 0 and 1, respectively. Next, principal component analysis (PCA) was
745 performed, from which the first 30 principal components (PCs) were selected for uniform manifold
746 approximation and projection (UMAP) analysis and cell clustering, which is a graph-based clustering
747 approach. Integration of the in vivo and in vitro samples was performed using the Seurat anchoring
748 method [80]. The integrated expression matrix was log-normalized and scaled. Next, PCA was performed
749 and the first 30 PCs were selected for UMAP analysis and cluster finding.
750 Marker genes for all clusters was detected as genes with at least Log2(fold change) ≥1 and adjusted P-
751 value ≤0.05 (Table S2). The GSEA MSigDB (https://www.gsea-msigdb.org/gsea/msigdb/) and Descartes
752 (https://descartes.brotmanbaty.org/bbi/human-gene-expression-during-

753 development/dataset/pancreas) databases were used to help assign identities for the 20 clusters
754 according to their marker genes.

755 **Table 3.** The number of cells in each sample and the total number of detected genes after data clean up

Sample	Cell number	Gene Number
E12	4,412	20,293
E14_B1	3,495	20,293
E14_B2	4,309	20,293
E17	2,241	20,293
PP_org	5056	20,293
PP+Matrigel	3485	20,293
PP+MP_B1	1456	20,293
PP+MP_B2	3602	20,293

756 **Inhibition of Wnt and Notch during aggregate preparation**
757 PP+MP aggregates were grown as detailed above with the following modifications to the organoid
758 medium:
759 1) After aggregation, the aggregates were grown in organoid medium without mouse R-spondin1
760 (Wnt activator) or in organoid medium without mouse R-spondin1 but supplemented with 10
761 µM Chiron (GSK3 inhibitor).
762 2) During the first 3 days AA, aggregates were grown in organoid medium. From day 4 AA until the
763 end of the differentiation, the aggregates were grown in organoid medium supplemented with
764 either 10 µM Chiron, 1 µM DAPT (γ-secretase and Notch signalling pathway inhibitor, Tocris
765 2634) or 1 µM XXI (Compound E, γ-secretase and Notch signalling pathway inhibitor, AdipoGen
766 Life Sciences AG-CR1-0081).
767 A total of 96 aggregates per condition were combined and averaged for RT-qPCR analysis.

768 **Mutual information between genes and clusters**
769 To characterize cluster 2, which was named 'proliferating cells', the similarity between the in vitro cells
770 in cluster 2 and all the clusters that contained embryonic cells (14 clusters), was assessed. Downstream
771 analysis was implemented with the entire set of qualified genes (20,293) rather than with the genes
772 restricted to the integration process (2,000 anchor genes). This step was performed as previously
773 detailed [41,82]. A mutual information (MI) technique [83] was used to select the informative genes related to
774 the embryonic clusters and the major in vitro clusters assembling the 'proliferating cells' cluster (4
775 clusters). The MI between the clusters (denoted as Y) and genes (denoted as X) was computed as
776 follows:
777 1. Calculation of cluster entropy:
778 $$(1)\ \ H(Y) = -\sum_{y=1:20} p(y)\log_2\big(p(y)\big),$$
779 where $p(y)$ is the probability of each cluster $y = 1, 2, \ldots 20$.
780
781 2. Discretization of the gene expression values into ten bins and calculation of the conditional
782 entropy $H(Y|X)$ as follows:
783 $$(2)\ H(Y|X) = \sum_x p(x)H(Y|X = x)\ ,$$

where $p(x)$ is the probability of the discretized gene expression across the cell population and $H(Y|X = x)$ is the cluster entropy given a specific gene expression value.

3. Computation of the MI between the clusters and each gene according to the equation below:

$$(3)\ MI(X;Y) = H(Y) - H(Y|X).$$

4. Setting of a threshold of the MI of all the genes and selection of the informative genes above this value (Fig. S8B).

Fig. S8B shows the MI between the genes and the clusters versus the number of genes. MI was set at 0.23, since at this point, the MI practically did not fluctuate with increments in gene number. This threshold, in which genes have MI above or equal to 0.23 (273 genes in total, Table S3), determines which genes are selected as input features for calculating the cosine similarity.

Cosine similarity

Cosine similarity was used as a measure of similarity between gene expression of the informative 273 genes selected by MI (Table S3) in one cluster versus another cluster. The cosine similarity was calculated as follows:

$$similarity = \frac{\sum_{i=1}^{n} A_i B_i}{\sqrt{\sum_{i=1}^{n} A_i^2}\sqrt{\sum_{i=1}^{n} B_i^2}},$$

where A and B represent two clusters and A_i and B_i are the gene expression values in each condition (n=273). Similarity of -1 indicates that the conditions are opposite and 1 indicates maximal similarity.

Aggregate embedding in gelatin

Gelatin hydrogel was covalently crosslinked with microbial transglutaminase (mTG) (MOO gloo TI transglutaminase, SKU:1203-50, modernist pantry) in the presence of calcium ions [64]. Porcine skin gelatin (300 g Bloom type A, Sigma-Aldrich, G1890) was dissolved in PBS 1X at 50 °C and immediately passed through a 0.22 µm filter. mTG was dissolved in 10 mM HEPES buffer (Biological Industries) supplemented with 100 mM $CaCl_2$ and sterilized by passing it through a 0.22µm filter.
On day 6 AA, PP+MP aggregates were embedded in 6.7% gelatin and 5% mTG, prewarmed to 37 °C. Plugs (50 µl) of gelatin-mTG with aggregates were pipetted into wells of a 24-well plate. To solidify the gelatin, the plate was incubated for 10 min at RT, followed by 30 min at 37 °C before the organoid medium was added.

Acknowledgments

We would like to thank Janette Zavin for assistance with staining, cell culture and image illustrations, and Rita Shuhmaher and Dina Safina for assistance with cell culture and fruitful discussion throughout the project. We would also like to express our sincere appreciation to Galia Ben David for her invaluable assistance throughout the project. We are grateful to Orit Bar-Am and Hagit Sason for their support in conducting the MTT assay, and Liat Linde and her team from the Technion Genomics Center for performing the 3D in vitro pancreatic aggregate single-cell RNA-sequencing. Images in Figures S1A were created with BioRender.com.

Funding

We acknowledge the support of the European Union's Horizon 2020 research and innovation programme Pan3DP FET Open [800981].
S. Edri is supported in part at the Technion by an Aly Kaufman Fellowship.

Author Contributions

Conceptualization: S.E. and S.L.; Methodology: S.E, N.S. and S.L.; Software: S.E.; Validation: S.E., V.R., O.G. and A.N.F.; Investigation: S.E., V.R. and O.G.; Resources: S.L.; Writing - original draft: S.E. and S.L.; Writing - review & editing: S.E., A.N.F., N.S., C.E.P. and S.L.; Supervision: S.L.; Funding acquisition: S.L. and C.E.P.

Competing interest

The authors declare that they have no competing interests.

Data and materials availability

All data needed to evaluate the conclusions in the paper are present in the paper and/or in the Supplementary Materials. The raw data for single-cell RNA sequencing of PP+MP aggregates (2 biological replicates), PP aggregates, and PP+Matrigel samples is accessible for download through the provided link:
https://data.mendeley.com/datasets/6hj6t5jgnc/draft?a=b2bcb3cb-16c3-45b7-b603-7270502e8f05

836 **References**

837 1. Villasenor, A., Chong, D. C., Henkemeyer, M. & Cleaver, O. Epithelial dynamics of pancreatic
838 branching morphogenesis. *Development* **137**, 4295–4305 (2010).

839 2. Balak, J. R. A., Juksar, J., Carlotti, F., Lo Nigro, A. & de Koning, E. J. P. Organoids from the Human
840 Fetal and Adult Pancreas. *Curr. Diab. Rep.* **19**, (2019).

841 3. Tam, P. P. . & Behringer, R. R. Mouse gastrulation: the formation of a mammalian body plan.
842 *Mech. Dev.* **68**, 3–25 (1997).

843 4. Ghezelayagh, Z. *et al.* Recapitulating pancreatic cell–cell interactions through bioengineering
844 approaches: the momentous role of non-epithelial cells for diabetes cell therapy. *Cell. Mol. Life*
845 *Sci. 2021* **1**, 1–26 (2021).

846 5. Ranjan, A. K., Joglekar, M. V & Hardikar, A. Endothelial cells in pancreatic islet development and
847 function. *Islets* (2009) doi:10.4161/isl.1.1.9054.

848 6. Jennings, R. E., Berry, A. A., Strutt, J. P., Gerrard, D. T. & Hanley, N. A. Human pancreas
849 development. *Development* **142**, 3126–3137 (2015).

850 7. Shih, H. P., Wang, A. & Sander, M. Pancreas Organogenesis: From Lineage Determination to
851 Morphogenesis. *http://dx.doi.org/10.1146/annurev-cellbio-101512-122405* **29**, 81–105 (2013).

852 8. Byrnes, L. E. *et al.* Lineage dynamics of murine pancreatic development at single-cell resolution.
853 *Nat. Commun. 2018 91* **9**, 1–17 (2018).

854 9. Prabakar, K. R. *et al.* Generation of Glucose-Responsive, Insulin-Producing Cells from Human
855 Umbilical Cord Blood-Derived Mesenchymal Stem Cells. *Cell Transplant.* **21**, 1321–1339 (2012).

856 10. Nostro, M. C. *et al.* Efficient Generation of NKX6-1+ Pancreatic Progenitors from Multiple Human
857 Pluripotent Stem Cell Lines. *Stem Cell Reports* **4**, 591–604 (2015).

858 11. Schaffer, A. E., Freude, K. K., Nelson, S. B. & Sander, M. Nkx6 Transcription Factors and Ptf1a
859 Function as Antagonistic Lineage Determinants in Multipotent Pancreatic Progenitors. *Dev. Cell*
860 **18**, 1022–1029 (2010).

861 12. Hohwieler, M. *et al.* Human pluripotent stem cell-derived acinar/ductal organoids generate
862 human pancreas upon orthotopic transplantation and allow disease modelling. *Gut* **66**, 473–486
863 (2017).

864 13. Rossi, G., Manfrin, A. & Lutolf, M. P. Progress and potential in organoid research. *Nature Reviews*
865 *Genetics* vol. 19 671–687 (2018).

866 14. Koike, H. *et al.* Modeling human hepato-biliary-pancreatic organogenesis from the foregut-
867 midgut boundary. *Nature* **574**, 112 (2019).

868 15. Nair, G. G. *et al.* Recapitulating endocrine cell clustering in culture promotes maturation of
869 human stem-cell-derived β cells. *Nat. Cell Biol.* **21**, 263–274 (2019).

870 16. Kim, Y. *et al.* Islet-like organoids derived from human pluripotent stem cells efficiently function in
871 the glucose responsiveness in vitro and in vivo. *Sci. Rep.* **6**, (2016).

872 17. Breunig, M. *et al.* Modelling Plasticity and Dysplasia of Pancreatic Ductal Organoids Derived from
873 Human Pluripotent Stem Cells. *Cell Stem Cell* **28**, 1105 (2021).

874 18. Huang, L. *et al.* Commitment and oncogene-induced plasticity of human stem cell-derived
875 pancreatic acinar and ductal organoids. *Cell Stem Cell* **28**, 1090-1104.e6 (2021).

876 19. Gonçalves, C. A. *et al.* A 3D system to model human pancreas development and its reference
877 single-cell transcriptome atlas identify signaling pathways required for progenitor expansion.
878 *Nat. Commun. 2021 121* **12**, 1–17 (2021).

879 20. Funata, M., Nio, Y., Erion, D. M., Thompson, W. L. & Takebe, T. The promise of human organoids
880 in the digestive system. *Cell Death Differ. 2020 281* **28**, 84–94 (2020).

881 21. Azzarelli, R. *et al.* Neurogenin3 phosphorylation controls reprogramming efficiency of pancreatic
882 ductal organoids into endocrine cells. *Sci. Rep.* **8**, (2018).

883 22. Huch, M. *et al.* Unlimited in vitro expansion of adult bi-potent pancreas progenitors through the
884 Lgr5/R-spondin axis. *EMBO J.* **32**, 2708–2721 (2013).

885 23. Greggio, C. *et al.* Artificial three-dimensional niches deconstruct pancreas development in vitro.
886 *Development* **140**, 4452–62 (2013).

887 24. Hughes, C. S., Postovit, L. M. & Lajoie, G. A. Matrigel: a complex protein mixture required for
888 optimal growth of cell culture. *Proteomics* **10**, 1886–1890 (2010).

889 25. Rezakhani, S., Gjorevski, N. & Lutolf, M. P. Low-Defect Thiol-Michael Addition Hydrogels as
890 Matrigel Substitutes for Epithelial Organoid Derivation. *Adv. Funct. Mater.* **30**, 2000761 (2020).

891 26. Cruz-Acuña, R. *et al.* Synthetic Hydrogels for Human Intestinal Organoid Generation and Colonic
892 Wound Repair. *Nat. Cell Biol.* **19**, 1326 (2017).

893 27. Gjorevski, N. *et al.* Designer matrices for intestinal stem cell and organoid culture. *Nature* **539**,
894 560–564 (2016).

895 28. Veres, A. *et al.* Charting cellular identity during human in vitro β-cell differentiation. *Nat. 2019*
896 *5697756* **569**, 368–373 (2019).

897 29. Smith, A. G. *et al.* Inhibition of pluripotential embryonic stem cell differentiation by purified
898 polypeptides. *Nature* **336**, 688–690 (1988).

899 30. Moreau, J.-F. *et al.* Leukaemia inhibitory factor is identical to the myeloid growth factor human
900 interleukin for DA cells. *Nature* **336**, 690–692 (1988).

901 31. Williams, R. L. *et al.* Myeloid leukaemia inhibitory factor maintains the developmental potential
902 of embryonic stem cells. *Nature* **336**, 684–687 (1988).

903 32. Ying, Q.-L. *et al.* The ground state of embryonic stem cell self-renewal. *Nature* **453**, 519–523
904 (2008).

905 33. Wray, J., Kalkan, T. & Smith, A. G. The ground state of pluripotency. *Biochem. Soc. Trans.* **38**,
906 1027–32 (2010).

907 34. Mulas, C. *et al.* Defined conditions for propagation and manipulation of mouse embryonic stem
908 cells. *Development* **146**, dev173146 (2019).

909 35. Delaspre, F. *et al.* Directed Pancreatic Acinar Differentiation of Mouse Embryonic Stem Cells via
910 Embryonic Signalling Molecules and Exocrine Transcription Factors. *PLoS One* **8**, e54243 (2013).

911 36. Borowiak, M. *et al.* Small Molecules Efficiently Direct Endodermal Differentiation of Mouse and
912 Human Embryonic Stem Cells. *Cell Stem Cell* **4**, 348–358 (2009).

913 37. Chen, S. *et al.* A small molecule that directs differentiation of human ESCs into the pancreatic
914 lineage. *Nat. Chem. Biol. 2009 54* **5**, 258–265 (2009).

915 38. Mamidi, A. *et al.* Mechanosignalling via integrins directs fate decisions of pancreatic progenitors.
916 *Nature* **564**, 114–118 (2018).

917 39. Fonseca, S. A. S., Costas, R. M. & Pereira, L. V. Searching for naïve human pluripotent stem cells.
918 *World J. Stem Cells* **7**, 649 (2015).

919 40. Morgani, S., Nichols, J. & Hadjantonakis, A.-K. The many faces of Pluripotency: in vitro
920 adaptations of a continuum of in vivo states. *BMC Dev. Biol.* **17**, 7 (2017).

921 41. Edri, S., Hayward, P., Jawaid, W. & Martinez Arias, A. Neuro-mesodermal progenitors (NMPs): a
922 comparative study between pluripotent stem cells and embryo-derived populations.
923 *Development* **146**, dev180190 (2019).

924 42. Edri, S., Hayward, P., Baillie-Johnson, P., Steventon, B. & Arias, A. M. An epiblast stem cell-derived
925 multipotent progenitor population for axial extension. *Development* **146**, dev.168187 (2019).

926 43. Tosolini, M. & Jouneau, A. From Naive to Primed Pluripotency: In Vitro Conversion of Mouse
927 Embryonic Stem Cells in Epiblast Stem Cells. in 209–216 (Humana Press, New York, NY, 2015).
928 doi:10.1007/7651_2015_208.

929 44. Glorieux, L. *et al.* Development of a 3D atlas of the embryonic pancreas for topological and
930 quantitative analysis of heterologous cell interactions. *Dev.* **149**, (2022).

931 45. Lammert, E., Cleaver, O. & Melton, D. Induction of pancreatic differentiation by signals from
932 blood vessels. *Science (80-.).* **294**, 564–567 (2001).

933 46. Konstantinova, I. & Lammert, E. Microvascular development: learning from pancreatic islets.
934 *BioEssays* **26**, 1069–1075 (2004).

935 47. Lammert, E., Cleaver, O. & Melton, D. Role of endothelial cells in early pancreas and liver
936 development. *Mech. Dev.* **120**, 59–64 (2003).

937 48. Pierreux, C. E. *et al.* Epithelial: Endothelial cross-talk regulates exocrine differentiation in
938 developing pancreas. *Dev. Biol.* **347**, 216–227 (2010).

939 49. Sharon, N. *et al.* A Peninsular Structure Coordinates Asynchronous Differentiation with
940 Morphogenesis to Generate Pancreatic Islets. *Cell* **176**, 790-804.e13 (2019).

941 50. Gouzi, M., Kim, Y. H., Katsumoto, K., Johansson, K. & Grapin-Botton, A. Neurogenin3 initiates
942 stepwise delamination of differentiating endocrine cells during pancreas development. *Dev. Dyn.*
943 **240**, 589–604 (2011).

944 51. Larsen, H. L. & Grapin-Botton, A. The molecular and morphogenetic basis of pancreas
945 organogenesis. *Semin. Cell Dev. Biol.* **66**, 51–68 (2017).

946 52. Pan, F. C. & Wright, C. Pancreas organogenesis: From bud to plexus to gland. *Dev. Dyn.* **240**, 530–
947 565 (2011).

948 53. Rukstalis, J. M. & Habener, J. F. Snail2, a mediator of epithelial-mesenchymal transitions,
949 expressed in progenitor cells of the developing endocrine pancreas. *Gene Expr. Patterns* **7**, 471–
950 479 (2007).

951 54. Tsuchiya, B., Sato, Y., Kameya, T., Okayasu, I. & Mukai, K. Differential expression of N-cadherin
952 and E-cadherin in normal human tissues. *Arch. Histol. Cytol.* **69**, 135–145 (2006).

953 55. Kim, S. Y. & Rane, S. G. The Cdk4-E2f1 pathway regulates early pancreas development by
954 targeting Pdx1+ progenitors and Ngn3+ endocrine precursors. *Development* **138**, 1903–1912
955 (2011).

956 56. Georgia, S., investigation, A. B.-T. J. of clinical & 2004, undefined. β cell replication is the primary
957 mechanism for maintaining postnatal β cell mass. *Am Soc Clin Investig*.

958 57. Kushner, J. A. *et al.* Cyclins D2 and D1 Are Essential for Postnatal Pancreatic β-Cell Growth. *Mol.*
959 *Cell. Biol.* **25**, 3752–3762 (2005).

960 58. Wu, Y. *et al.* Hippo Signaling Pathway in Pancreas Development. *Front. Cell Dev. Biol.* **9**, 1132
961 (2021).

962 59. McCracken, K. W. & Wells, J. M. Molecular Pathways Controlling Pancreas induction. *Semin. Cell*
963 *Dev. Biol.* **23**, 656 (2012).

964 60. Young, T. *et al.* Cdx and Hox genes differentially regulate posterior axial growth in mammalian
965 embryos. *Dev. Cell* **17**, 516–26 (2009).

966 61. Deschamps, J. & Duboule, D. Embryonic timing, axial stem cells, chromatin dynamics, and the
967 Hox clock. *Genes Dev.* **31**, 1406–1416 (2017).

968 62. Kuo, T. L., Cheng, K. H., Chen, L. T. & Hung, W. C. Deciphering The Potential Role of Hox Genes in
969 Pancreatic Cancer. *Cancers (Basel).* **11**, (2019).

970 63. Larsen, B. M., Hrycaj, S. M., Newman, M., Li, Y. & Wellik, D. M. Mesenchymal Hox6 function is

971 required for mouse pancreatic endocrine cell differentiation. *Dev.* **142**, 3859–3868 (2015).

972 64. Gupta, D., Santoso, J. W. & McCain, M. L. Characterization of Gelatin Hydrogels Cross-Linked with
973 Microbial Transglutaminase as Engineered Skeletal Muscle Substrates. *Bioeng. (Basel,*
974 *Switzerland)* **8**, 1–16 (2021).

975 65. Paguirigan, A. L. & Beebe, D. J. Protocol for the fabrication of enzymatically crosslinked gelatin
976 microchannels for microfluidic cell culture. *Nat. Protoc. 2007 27* **2**, 1782–1788 (2007).

977 66. Yung, C. W. *et al.* Transglutaminase crosslinked gelatin as a tissue engineering scaffold. *J. Biomed.*
978 *Mater. Res. Part A* **83A**, 1039–1046 (2007).

979 67. McCain, M. L., Agarwal, A., Nesmith, H. W., Nesmith, A. P. & Parker, K. K. Micromolded Gelatin
980 Hydrogels for Extended Culture of Engineered Cardiac Tissues. *Biomaterials* **35**, 5462 (2014).

981 68. Kleeff, J. *et al.* Altered expression and localization of the tight junction protein ZO-1 in primary
982 and metastatic pancreatic cancer. *Pancreas* **23**, 259–265 (2001).

983 69. Lee, D. H. & Chung, H. M. Differentiation into Endoderm Lineage: Pancreatic differentiation from
984 Embryonic Stem Cells. *Int. J. Stem Cells* **4**, 35 (2011).

985 70. Ma, X. *et al.* Human expandable pancreatic progenitor-derived β cells ameliorate diabetes. *Sci.*
986 *Adv.* **8**, (2022).

987 71. Sneddon, J. B., Borowiak, M. & Melton, D. A. Self-renewal of embryonic-stem-cell-derived
988 progenitors by organ-matched mesenchyme. *Nature* **491**, 765–768 (2012).

989 72. Heymans, C., Degosserie, J., Spourquet, C. & Pierreux, C. E. Pancreatic acinar differentiation is
990 guided by differential laminin deposition. *Sci. Reports 2019 91* **9**, 1–13 (2019).

991 73. Veenvliet, J. V. *et al.* Mouse embryonic stem cells self-organize into trunk-like structures with
992 neural tube and somites. *Science* **370**, (2020).

993 74. Rahman, A. *et al.* Extracellular matrix flow guides in-vitro epithelial morphogenesis. *bioRxiv*
994 2022.10.21.513217 (2022) doi:10.1101/2022.10.21.513217.

995 75. Li, X. Y., Zhai, W. J. & Teng, C. B. Notch Signaling in Pancreatic Development. *Int. J. Mol. Sci.* **17**,
996 (2016).

997 76. Sharon, N. *et al.* Wnt Signaling Separates the Progenitor and Endocrine Compartments during
998 Pancreas Development. *Cell Rep.* **27**, (2019).

999 77. Liu, Z., Tanabe, K., Bernal-Mizrachi, E. & Permutt, M. A. Mice with beta cell overexpression of
1000 glycogen synthase kinase-3β have reduced beta cell mass and proliferation. *Diabetologia* **51**,
1001 623–631 (2008).

1002 78. Grebenyuk, S. & Ranga, A. Engineering Organoid Vascularization. *Front. Bioeng. Biotechnol.* **7**,
1003 (2019).

1004 79. Talavera-Adame, D. & Dafoe, D. C. Endothelium-derived essential signals involved in pancreas
1005 organogenesis. *World J. Exp. Med.* **5**, 40 (2015).

1006 80. Hao, Y. *et al.* Integrated analysis of multimodal single-cell data. *Cell* **184**, 3573-3587.e29 (2021).

1007 81. Loza, M., Teraguchi, S., Standley, D. M. & Diez, D. Unbiased integration of single cell
1008 transcriptome replicates. *NAR Genomics Bioinforma.* **4**, (2022).

1009 82. Vanitha, C. D. A., Devaraj, D. & Venkatesulu, M. Gene Expression Data Classification Using
1010 Support Vector Machine and Mutual Information-based Gene Selection. *Procedia Comput. Sci.*
1011 **47**, 13–21 (2015).

1012 83. Battiti, R. Using mutual information for selecting features in supervised neural net learning. *IEEE*
1013 *Trans. Neural Networks* **5**, 537–550 (1994).

1014